

Linear control of oscillator and amplifier flows*Peter J. Schmid^{1,†} and Denis Sipp^{2,‡}¹*Department of Mathematics, Imperial College London, London SW7 2AZ, United Kingdom*²*ONERA, DAFE, 8 Rue des Vertugadins, F-92190 Meudon, France*

(Received 3 February 2016; published 30 August 2016)

Linear control applied to fluid systems near an equilibrium point has important applications for many flows of industrial or fundamental interest. In this article we give an exposition of tools and approaches for the design of control strategies for globally stable or unstable flows. For unstable oscillator flows a feedback configuration and a model-based approach is proposed, while for stable noise-amplifier flows a feedforward setup and an approach based on system identification is advocated. Model reduction and robustness issues are addressed for the oscillator case; statistical learning techniques are emphasized for the amplifier case. Effective suppression of global and convective instabilities could be demonstrated for either case, even though the system-identification approach results in a superior robustness to off-design conditions.

DOI: [10.1103/PhysRevFluids.1.040501](https://doi.org/10.1103/PhysRevFluids.1.040501)**I. INTRODUCTION**

Many fluid devices of technological or fundamental importance are limited in their operational range by instabilities or sensitivities. Instabilities in a laminar boundary layer can cause a transition to turbulence and consequently increase drag and heat transfer on aircrafts [1–4]; reactive-flow instabilities [5] can give rise to nonstoichiometric combustion and thus increase the output of environmentally harmful side products; thermoacoustic instabilities in combustion chambers can lead to strong vibrations and material fatigue [6,7]; magnetically induced instabilities in tokamak configurations can be detrimental to sustaining the plasma fusion process [8,9]; the onset of vortex-induced vibrations can bring about substantial damage to flexible structures [10,11]. These examples are but a few that illustrate the need for and potential benefit of controlling instabilities in advanced fluid devices. Quests for more performance, less drag, increased safety margins, unexplored parameter regimes, and diminished environmental impact can only be answered by changing the innate flow behavior of fluid systems. Some of these quests can be achieved with improved designs, judicious modifications, localized roughness, or other passive devices [12]; some quests need a simple forcing of the flow at a given frequency. Yet other quests require adaptive control based on information gained from the flow about the current state [13–15]. This latter approach is the topic of this article.

Since the inherent flow behavior has to be changed, it seems intuitive that different flow behaviors call for different control techniques and setups. As we will see in what follows, the most critical component in the design of control strategies is the response to uncertainty and noise. What can be controlled in a clean and numerically controlled noise environment may fail to achieve the same results in an experimental setting where unidentified or unidentifiable noise sources have not been incorporated into the control design.

Physically, noise and uncertainty can arise from different sources: Turbulent fluctuations in the freestream, acoustic waves, wall roughness, or imposed frequencies from secondary sources (due to separation, from a pump or other measuring equipment, etc.) are but a few examples that may

*This paper is based on an invited lecture given by Peter J. Schmid at the 65th Annual Meeting of the APS Division of Fluid Dynamics, which was held 18–20 November 2012 in San Diego (CA), USA.

†pjschmid@imperial.ac.uk

‡sipp@onera.fr

disrupt a control design that has not included these influences in its setup. Besides these physical error sources, we also have to be aware of modeling errors. They manifest themselves, for example, in flow effects not accounted for by our governing equations, in design assumptions that are only approximately valid in our application, in mean and base profiles that fluctuate stochastically, and parameters and input fields that can only be measured or determined within a specific tolerance. Regardless of their origin or type, these errors and uncertainties propagate through the model, which underlies the control design and impact its layout and ultimately its performance and robustness.

In the design of linear active flow control strategies, we distinguish two distinct flow behaviors: noise amplifiers and oscillators. Oscillators are characterized by the presence of a global instability that dominates the flow. Our goal is the suppression of this instability and the return of the compensated system to the linearly stable regime [16,17]. Due to the dominance of an instability on the measurements we take from the flow, noise-related issues in the control design, although present, play a somewhat subordinate role: They are not critical, but are nonetheless important. The latter statement holds for modeling errors as well. In the case of oscillators then, an approach based on postulating governing equations with a rudimentary model for the noise environment appears sufficient for an effective design of a compensator, as long as the dominant instabilities of the system have been modeled appropriately. Flow control for stabilizing the shear layer over cavities [16,18] or the wake of blunt bodies (such as cylinders) has shown success following this approach. Amplifier flows represent the second category and are far more challenging to control. In this case, no global stability is present in the flow and perturbations are typically amplified locally, as they are convected downstream by the flow. In the absence of a dominant unstable structure, the flow reacts sensitively to incoming perturbations and the general noise environment. Modeling this type of behavior thus critically depends on how well and accurately this noise environment can be captured. It is not difficult to imagine that this issue poses a far greater challenge, when contrasted with oscillator flows. Even if the incoming perturbations could be measured with sufficient accuracy, there still remains the important matter of modeling errors and parameter uncertainties.

Due to their different response behavior to external noise, it should not come as a surprise that oscillator and amplifier flows require different approaches for an effective control design. The distinction concerns not only the actual control design procedure, but also the control setup, i.e., where to place the sensor(s), where to place the actuator(s), is crucially affected by the type of flow we wish to manipulate.

II. TWO GENERIC FLOW BEHAVIORS: ONE MODEL

During the course of this article we will cover the control design steps for oscillator and amplifier flows, pointing out challenges and particularities in their analysis and control. As a typical oscillator flow, we consider the open flow over a square cavity at supercritical Reynolds numbers (in our case $Re = 7500$). The geometric configuration is sketched in Fig. 1(a). The shear layer forming on top of the cavity becomes unstable for Reynolds numbers (based on the freestream velocity and the cavity depth) above $Re = 4140$, rendering the flow globally unstable [19]. In the same sketch we also indicate the control setup for this flow. An actuator u is placed upstream near the cavity edge, while sensors are placed at three locations: a sensor s upstream of the actuator (to gain information about the incoming disturbance field w), a sensor y near the downstream edge of the cavity (providing information about the general flow behavior, in particular about the instability), and a sensor z farther downstream (to evaluate a cost objective). For our specific case, the actuator consists of a localized region of vertical velocity near the wall, imposed as a volume force in the corresponding momentum equation, while the sensors record the wall-shear stress, again over a localized region.

As an example for an amplifier flow, we introduce the flow over a backward-facing step at a Reynolds number (based on the step height) of $Re = 500$, as sketched in Fig. 1(b). Past the step a separation zone forms that, just as in the case of the cavity, recirculates fluid upstream where it again interacts with the oncoming flow. The two-dimensional flow over a backward-facing step is globally stable and thus qualifies as an example of a noise amplifier [20]. The setup for controlling this flow

LINEAR CONTROL OF OSCILLATOR AND AMPLIFIER FLOWS

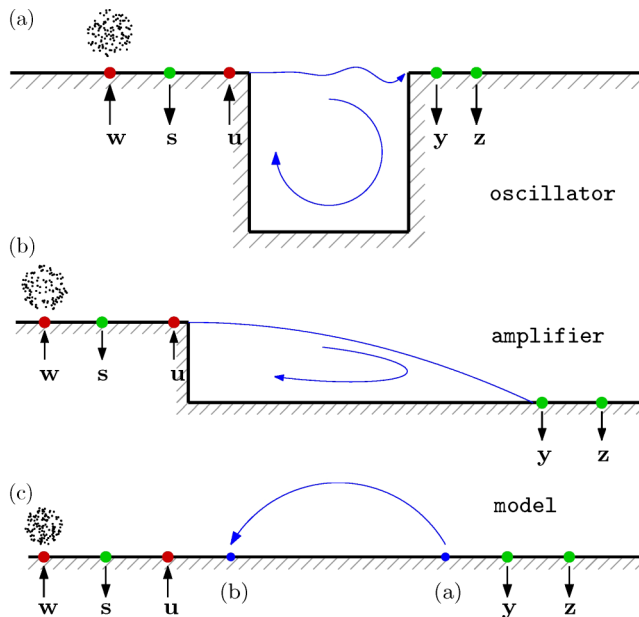


FIG. 1. Sketch of typical flow control configurations for (a) flow over a square cavity, representing an oscillator flow, and (b) flow over a backward-facing step, representing an amplifier flow. A single actuator u and upstream noise source w constitute the input to the system; the upstream and downstream sensors s and y , respectively, together with the performance sensor z constitute the output from the system. (c) Sketch of a simplified model, consisting of equivalent input and output devices and a system-specific feedback of variable strength.

is identical to the one introduced for the cavity: Noise w introduced upstream passes the upstream sensor s and the actuator u before impacting the downstream sensor y (in our case, placed near the base-flow reattachment location); a final sensor z is placed farther downstream, its purpose being the evaluation of the cost objective and thus the success and performance of our control effort. As before, we consider an actuator, which imposes a localized source of vertical momentum near the wall, and a sensor, which detects shear information over a localized region of the wall.

Even though the two configurations represent two rather distinct flow behaviors, they also show a large degree of similarity. Both flows (i) are subject to upstream noise w , (ii) are convectively dominated by a base flow from left to right, and (iii) show a localized region where information propagates upstream (in the cavity and the separation bubble, respectively) to interact with the oncoming flow (near the upstream edge of the cavity and the step, respectively). The distinguishing feature of the two flows, which labels them as oscillators or amplifiers, appears to be the strength of the internal feedback: If it is strong enough to cause in-place amplification at at least one point of the flow domain, a global instability ensues; if the internal feedback is insufficient to cause amplification, we have a globally stable flow.

In an attempt to reduce the two generic shear flows to an even simpler model equation we propose and introduce a discrete model [21] that captures the main features of either flow and uses the strength of the internal feedback to switch from amplifier to oscillator behavior. The model consists of a state vector with a finite number of components, among them the input location of the upstream noise w , the three sensor locations (for s , y , and z), and the actuator location u . In addition, two locations [indicated by (a) and (b) in Fig. 1(c)] are introduced that will be used to enforce a link between downstream and upstream positions in the flow. For our analysis, we choose a state vector with 12 components, yielding a 12-dimensional system; the layout of the state vector components is indicated below in Fig. 2.

PETER J. SCHMID AND DENIS SIPP

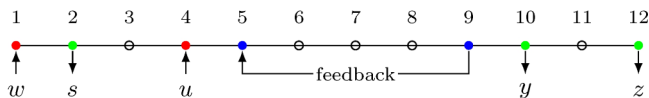


FIG. 2. Layout of the 12-component state vector for the model system, describing the configuration depicted in Fig. 1(c).

In mathematical terms, we use a time-discrete formulation and describe a mapping of the state vector $\mathbf{q} = (q_1, \dots, q_{12})^T$ over a fixed time-unit based on the following set of equations:

$$\mathbf{q}_{n+1} = \mathbf{A}\mathbf{q}_n + \mathbf{B}u_n + \mathbf{B}_w w_n, \quad (1a)$$

$$\mathbf{y}_n = \mathbf{C}_y \mathbf{q}_n, \quad (1b)$$

$$z_n = \mathbf{C}_z \mathbf{q}_n. \quad (1c)$$

The column vector \mathbf{q} contains the 12 components that fully describe the state of the system. Following the design of Figs. 1(c) and 2 we take the system, control, noise, and measurement matrices as

$$\mathbf{A} = \begin{pmatrix} 0 & & & & & & & & & & & \\ 1 & 0 & & & & & & & & & & \\ & 1 & 0 & & & & & & & & & \\ & & 1 & 0 & & & & & & & & \\ & & & 1 & 0 & & & & & & & \\ & & & & 1 & 0 & & & & & & \\ & & & & & 1 & 0 & & & & & \\ & & & & & & 1 & 0 & & & & \\ & & & & & & & 1 & 0 & & & \\ & & & & & & & & 1 & 0 & & \\ & & & & & & & & & 1 & 0 & \\ & & & & & & & & & & 1 & 0 \end{pmatrix}, \quad \mathbf{B} = \begin{pmatrix} 0 \\ 0 \\ 0 \\ 1 \\ 0 \\ 0 \\ 0 \\ 0 \\ 0 \\ 0 \\ 0 \\ 0 \end{pmatrix},$$

$$\mathbf{B}_w = \begin{pmatrix} 1 \\ 0 \\ 0 \\ 0 \\ 0 \\ 0 \\ 0 \\ 0 \\ 0 \\ 0 \\ 0 \\ 0 \end{pmatrix}, \quad \mathbf{C}_y^T = \begin{pmatrix} 0 & 0 \\ 1 & 0 \\ 0 & 0 \\ 0 & 0 \\ 0 & 0 \\ 0 & 0 \\ 0 & 0 \\ 0 & 0 \\ 0 & 0 \\ 0 & 1 \\ 0 & 0 \\ 0 & 0 \end{pmatrix}, \quad \mathbf{C}_z^T = \begin{pmatrix} 0 \\ 0 \\ 0 \\ 0 \\ 0 \\ 0 \\ 0 \\ 0 \\ 0 \\ 0 \\ 0 \\ 1 \end{pmatrix}. \quad (2)$$

Matrix entries that are not specified are taken as zero. The system matrix \mathbf{A} describes pure advection (with the subdiagonal matrix entries performing a lossless shift operation) and the matrix entry $\mathbf{A}_{5,9}$ provides an opportunity to introduce feedback from a downstream position q_9 to an upstream position q_5 , mimicking the transport of information via the cavity or separation bubble. The remaining matrices describe input (\mathbf{B} and \mathbf{B}_w) or output (\mathbf{C}_y and \mathbf{C}_z) details; see Fig. 2. It is easily verified that the system, described by the matrix \mathbf{A} , becomes unstable as the absolute value of the feedback coefficient b exceeds unity. In the case of an instability, with $|b| > 1$, there are five unstable eigenvalues and the associated eigenfunctions show support between the fifth position and the right edge of the domain, i.e., $\tilde{\mathbf{q}} = (0 \ 0 \ 0 \ 0 \ \times \ \times \ \dots \ \times)^T$, with a peak at the fifth location followed by a “wake” farther

LINEAR CONTROL OF OSCILLATOR AND AMPLIFIER FLOWS

downstream; this is reminiscent of fluid systems with a spatially limited amplification zone. The remaining seven eigenvalues are zero with associated eigenfunctions that show a nonzero component only in the rightmost, 12th position; they are associated with pure advection and related to boundary modes [22].

Dissipative (amplification) effects (certainly present in the two flow configurations) will be neglected in this model, as it is argued that, for our purpose, added dissipation (amplification) simply requires a larger (smaller) feedback strength to generate the equivalent flow behavior. The feedback strength in the model thus should be interpreted as the effective, dissipation-(amplification)-corrected feedback present in the two flow configurations.

The above simplified model will be used to guide us towards an effective setup of control problems for oscillator and amplifier flows.

III. CONTROL SETUP

The sketches of the flow configurations and model considered in this article already present a first impression of a typical flow control setup; we will further elaborate on this in what follows.

The motion of the fluid is fully described by the state vector \mathbf{q} , which describes the evolution of perturbations about an equilibrium state \mathbf{q}_0 . For sufficiently small amplitudes, this evolution can be described by linearized equations. This linearized model is subjected to an input signal, describing the action of our controller, and supplemented by an output signal, representing a measurement taken by a sensor. To account for the noise environment and uncertainties, as well as for the contamination of the sensor signal, we append two stochastic terms to the governing equations. This setup has to be augmented by a final measurement, taken from the system, whose norm acts as a performance measure for our control efforts.

Mathematically, the above layout of the control problem reads (in continuous-time form)

$$\dot{\mathbf{q}} = \mathbf{A}\mathbf{q} + \mathbf{B}u + \mathbf{B}_w w, \quad (3a)$$

$$\mathbf{y} = \mathbf{C}_y \mathbf{q} + \mathbf{g}, \quad (3b)$$

$$z = \mathbf{C}_z \mathbf{q}. \quad (3c)$$

In the above equation, the system matrix \mathbf{A} expresses the inherent dynamics of the perturbations, \mathbf{B} describes the manner in which a control signal u acts on the fluid system (which contains information about the location and type of control), \mathbf{C}_y includes information about the measurements taken from the system (again, in location and type), and \mathbf{C}_z contains the manner in which we choose to evaluate the system. Even though z can also be considered an output from the system, we make a distinction between true measurements s and y that are fed back to establish control and the signal z that merely enters into a cost objective \mathcal{J} . The two stochastic noise sources w and \mathbf{g} respectively influence the evolution of the perturbations via \mathbf{B}_w or contaminate the measurements directly.

The cost objective \mathcal{J} quantifies our goal of applying a control strategy: For oscillator flows, this is commonly the suppression of global instabilities, while for amplifier flows, it is the suppression of environmental noise amplified by the system. This cost objective is often augmented by a second term that takes into account the energy of the exerted control effort. Inclusion of this term avoids excessive injection of control energy into the flow to reach our objective. While the first part quantifies the (raw) performance of our control strategy, the second part penalizes the amount of control energy to reach this performance. A balance has to be struck between these two counteracting components of the cost objective.

The goal of our flow control problem is to translate measurements taken from the flow (i.e., \mathbf{y}) into a control strategy u such that our cost objective \mathcal{J} is rendered optimal. The resulting optimization problem has to be solved while observing the governing equations (3).

PETER J. SCHMID AND DENIS SIPP

This optimization can be accomplished in two stages [13]. First, Eq. (3b) is ignored (as are error terms) and a controller of the form $u = \mathbf{K}\mathbf{q}$ is assumed, which yields

$$\dot{\mathbf{q}} = \mathbf{A}\mathbf{q} + \mathbf{B}\mathbf{K}\mathbf{q}, \quad (4a)$$

$$z = \mathbf{C}_z\mathbf{q}. \quad (4b)$$

This assumption results in what is referred to as the full state-information control (FSC) design. We choose our cost objective in the form $\int_0^\infty |z|^2 + \ell^2|u|^2 dt$, which includes both our performance measure z and a measure of our expended control u . The parameter ℓ , balancing these two components, is user defined and can be used to penalize or encourage control efforts. Optimizing our cost objective subject to the above closed-loop equation yields an algebraic Riccati equation from which the control gain \mathbf{K} can be determined that optimally accomplishes our control objective.

Our assumption of access to the full state \mathbf{q} is the concern of the second stage of the control design, as only the measurements s, y are available for our control effort. An estimator that reconstructs an approximation to the state \mathbf{q} solely from available measurements s, y has to be constructed. The estimated state and measurements are denoted by carets, e.g., $\hat{\mathbf{q}}$ and $\hat{\mathbf{y}}$. This estimator is governed by the identical system, control, and measurement matrices from Eqs. (3), with all error terms ignored, but (3a) is augmented by an additional driving term of the form $-\mathbf{L}(\mathbf{y} - \hat{\mathbf{y}})$, which takes into account discrepancies between the true measurement \mathbf{y} and the estimated measurement $\hat{\mathbf{y}}$ to force the estimated state $\hat{\mathbf{q}}$ towards the true (inaccessible) state \mathbf{q} . We have

$$\dot{\hat{\mathbf{q}}} = \mathbf{A}\hat{\mathbf{q}} + \mathbf{B}u - \mathbf{L}(\mathbf{y} - \hat{\mathbf{y}}), \quad (5a)$$

$$\hat{\mathbf{y}} = \mathbf{C}_y\hat{\mathbf{q}}, \quad (5b)$$

$$\mathbf{e} = \mathbf{q} - \hat{\mathbf{q}}. \quad (5c)$$

The underlying assumption is that a small mismatch in the measurement signals coincides with a minimal mismatch between the estimated and true states. The manner in which measurement discrepancies are accounted for is determined by \mathbf{L} , referred to as the Kalman gain. This gain results from a second optimization problem: This time the performance measurement is equivalent to the estimation error field \mathbf{e} , i.e., the difference between the true state \mathbf{q} and the estimated state $\hat{\mathbf{q}}$. Minimizing $\|\mathbf{e}\|$ subject to satisfying the governing equation for the estimator yields, again, an algebraic Riccati equation; its solution determines, via an algebraic expression, the optimal Kalman gain \mathbf{L} .

In the design of the estimator and the calculation of the Kalman gain \mathbf{L} the noise environment plays a big role. In particular, the ratio of \mathbf{G} to \mathbf{W} determines the effectiveness of the estimator in recovering state information from noise-corrupted measurements. In this ratio, \mathbf{G} stands for the covariance of the signal noise g , while \mathbf{W} represents the covariance of the incoming noise w . Large ratios of \mathbf{G}/\mathbf{W} indicate highly corrupted signals with little information about the true measurement. Low ratios, on the other hand, are evidence of a clean uncorrupted signal that the estimator can use to approximately reconstruct the state vector $\hat{\mathbf{q}}$. As we will see below, the performance of the estimator and, consequently of the compensator, crucially depends on the ratio \mathbf{G}/\mathbf{W} .

Once the estimated state $\hat{\mathbf{q}}$ is recovered from the measurements \mathbf{y} , it is used in place of the true state \mathbf{q} in the controller, i.e., we implement the control strategy $u = \mathbf{K}\hat{\mathbf{q}}$. The control gain \mathbf{K} is still optimal, even if it is used with the estimated rather than the true state. This property, referred to as the separation principle, can be easily deduced by formulating a governing equation for the state estimation error $\mathbf{e} = \mathbf{q} - \hat{\mathbf{q}}$, which is independent of the true state \mathbf{q} . We obtain

$$\dot{\mathbf{e}} = \mathbf{A}\mathbf{e} + \mathbf{B}u + \mathbf{B}_w w, \quad (6a)$$

$$\mathbf{y} = \mathbf{C}_y\mathbf{e}, \quad (6b)$$

$$z = \mathbf{C}_z\mathbf{e}, \quad (6c)$$

LINEAR CONTROL OF OSCILLATOR AND AMPLIFIER FLOWS

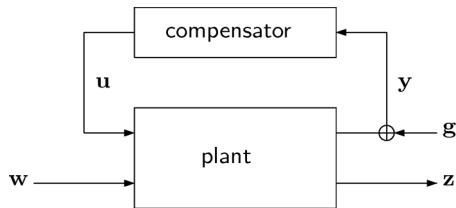


FIG. 3. Block diagram of a typical feedback control setup, including plant, compensator, external noise sources (\mathbf{w}, \mathbf{g}), and objective output z .

$$\dot{\mathbf{e}} = (\mathbf{A} + \mathbf{L}\mathbf{C}_y)\mathbf{e} + \mathbf{B}_w w - \mathbf{L}y, \tag{6d}$$

$$u = \mathbf{K}\hat{\mathbf{q}}. \tag{6e}$$

Combining the estimator and controller into a compensator and applying it to the fluid system provides an optimal control strategy that accomplishes our set objective. The entire control setup is displayed in Fig. 3 in the form of a block diagram. Considering this setup from a purely control-theoretic viewpoint, it is evident from the figure that the configuration represents *output feedback control* for each case (oscillator and amplifier), as the control is reintroduced into the fluid system. A distinction of *disturbance feedforward* and *disturbance feedback* can be made, respectively, for amplifiers and oscillators.

IV. WHAT CAN WE LEARN FROM OUR SIMPLE MODEL?

Before launching into the control design for amplifier and oscillator flows, we consider our simplified 12-dimensional model introduced in the previous section. To this end, we employ the above procedures and design feedback control schemes for our system for the distinct cases of oscillator ($|b| > 1$) and amplifier ($|b| < 1$) behavior. In addition, we consider distinguishing limits for the controller as well as the estimator. We are particularly interested in the closed-loop performance of the compensated system (with estimator and controller attached) in these limits and in the associated flow of relevant information from the sensors to the actuator. As a performance measure, we take the norm of the transfer function linking the upstream noise w to the downstream sensor z , with the system in a closed-loop feedback state; a performing compensator will successfully reduce the transfer function, compared to the uncontrolled configuration. The layout for our analysis is illustrated in the sketch in Fig. 4; the results of our analysis are tabulated in Fig. 5.

A. Oscillator behavior

Globally unstable flows, in our case enforced by setting the intrinsic feedback parameter to $b = 1.1$, results in oscillatory flow behavior. Following the two-stage control design procedure, we first determine the control gain \mathbf{K} for a full-state information setting by solving an algebraic

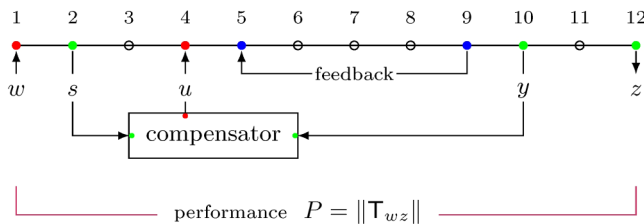


FIG. 4. Sketch of the 12-dimensional closed-loop feedback system, indicating the input and output ports, the system-internal feedback, the user-designed compensator, and the performance measure.

PETER J. SCHMID AND DENIS SIPP

oscillator flow (globally unstable)			amplifier flow (globally stable)	
uncontrolled performance $P = \ \mathbf{T}_{zw}\ = \infty$			uncontrolled performance $P = \ \mathbf{T}_{zw}\ = 1$	
Controller	$\ell \gg 1$ (SGL)	$\ell \ll 1$ (LGL)	Controller	$\ell \ll 1$ (LGL)
FSC	$P = 1.984$	$P = 0$	FSC	$P = 0$
Estimator (PSC)			Estimator (PSC)	
$G \gg W$ (SGL)			$G \gg W$ (SGL)	
$\begin{bmatrix} s \\ y \end{bmatrix}$	[failure]	[failure]	$\begin{bmatrix} s \\ y \end{bmatrix}$	$P = 1$ [no action]
$\begin{bmatrix} s \\ y \end{bmatrix}$	$P = 5.489$	$P = 2.823$	$\begin{bmatrix} s \\ y \end{bmatrix}$	$P = 1$ [no action]
$\begin{bmatrix} s \\ y \end{bmatrix}$	$P = 5.489$	$P = 2.823$	$\begin{bmatrix} s \\ y \end{bmatrix}$	$P = 1$ [no action]
$G \ll W$ (LGL)			$G \ll W$ (LGL)	
$\begin{bmatrix} s \\ y \end{bmatrix}$	[failure]	[failure]	$\begin{bmatrix} s \\ y \end{bmatrix}$	$P = 0$ (FSC)
$\begin{bmatrix} s \\ y \end{bmatrix}$	$P = 2.82$	$P = 1.487$	$\begin{bmatrix} s \\ y \end{bmatrix}$	$P = 1$ [no action]
$\begin{bmatrix} s \\ y \end{bmatrix}$	$P = 1.984$ (FSC)	$P = 0$ (FSC)	$\begin{bmatrix} s \\ y \end{bmatrix}$	$P = 0$ (FSC)

FIG. 5. Summary of performance analysis for the FSC and the estimator in various gain limits and input configurations (see the text for explanation). On the left is oscillator flow with the feedback parameter chosen as $b = 1.1$, yielding a globally unstable condition. On the right is amplifier flow with a feedback parameter set to $b = 0$.

discrete Riccati equation. For this case, we have to decide on the user-specified parameter ℓ , which determines the amount of expended control efforts. In the limit of $\ell \rightarrow \infty$, control is applied rather parsimoniously, as any control effort is drastically penalized in the optimization problem. As a result, the control gains are rather small and any control effort is limited to doing the most necessary to stabilize the unstable system. This limit is referred to as the small-gain limit (SGL). Owing to this minimal control effort, the performance is restricted as a consequence. Measured by the norm of the closed-loop transfer function, i.e., $\|\mathbf{T}_{wz}\|$, the performance in this limit is $P = 1.984$, which will serve as a reference value for other cases and the partial state-information control (PSC). In the limit of $\ell \rightarrow 0$, we apply control far more liberally; as a result, the control gains \mathbf{K} become rather large and this limit is referred to as the large-gain limit (LGL). In this limit, with full-state information available to the controller and no limitations imposed on the control effort, the performance is ideal with $P = 0$, i.e., the instabilities are not only weakened, but entirely eliminated.

It is instructive to assess the shape of the control gain \mathbf{K} , which indicates from which positions the optimal controller extracts the information necessary to control the flow. In our case, the control gain \mathbf{K} has only two nonzero entries: immediately upstream of the actuator (third position, to target the incoming perturbations using opposition control) and at the downstream edge of the feedback loop (eighth position). We thus have $\mathbf{K} = (0 \ 0 \ \alpha \ 0 \ 0 \ 0 \ 0 \ \beta \ 0 \ 0 \ 0 \ 0)$, with α and β as (negative) entries. The relative weight of the control gain entries α, β is displayed in Fig. 6 as a function of the feedback strength b . As we change from a mildly unstable flow ($b \gtrsim 1$) to a strong feedback-generated instability ($b = 5$), the relative weights tend from an equal consideration of the two input signals towards an increasing preference of the downstream edge of the feedback loop for the information that is passed to the full-state information controller. In other words, the stronger the instability, the less we have to concern ourselves with the details of the incoming disturbance environment.

We proceed with the second stage of the design: the development and incorporation of an estimator into the feedback loop. Only the two signals s and y are taken into account, from which the flow state $\hat{\mathbf{q}}$ is estimated. For oscillator flows to be successfully compensated, it is imperative that the estimator detects and recovers the unstable modes from the measurements. We have seen above that all unstable modes have a particular shape, with support only downstream of the intrinsic feedback loop (in our case, starting at the fifth position). For this reason, estimating the instabilities from the s sensor upstream must result in failure, since all unstable modes are unobservable by s . This is

LINEAR CONTROL OF OSCILLATOR AND AMPLIFIER FLOWS

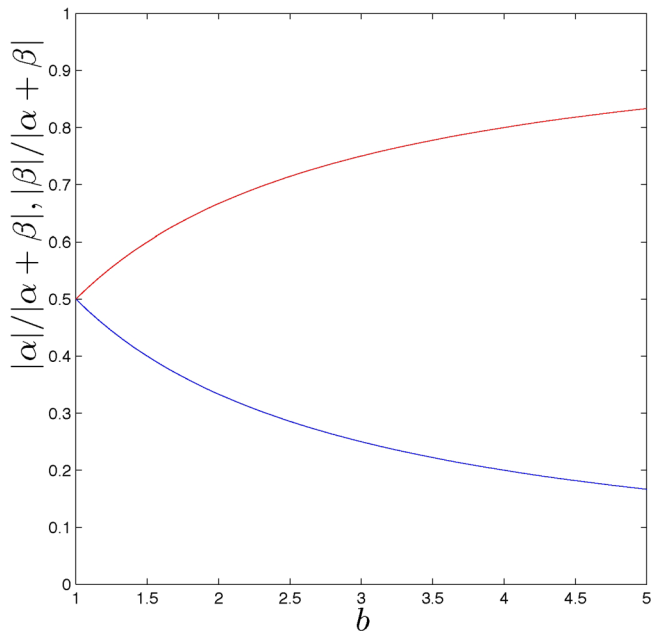


FIG. 6. Relative control gain versus the strength of the internal feedback—downstream control gain (in red) and upstream control gain (in blue)—for the small-gain limit.

confirmed when solving the Riccati equation to determine the Kalman gain L for the sensor location s : No solution can be found.

Using an input signal from the downstream sensor y for the estimation of the unstable modes yields an optimal Kalman gain L from the algebraic Riccati equation, which, coupled to the optimal controller, achieves a satisfactory performance result. At this point, we have to distinguish two limits for the estimator. (i) In the first limit, we assume a highly corrupted measurement signal (indicated by $G \gg W$) that causes the estimator to react rather reluctantly to detected measurement discrepancies. This limit is known as the small-gain limit for the Kalman gain L . In the second limit, the noise variance in the measurements is very small (i.e., $G \ll W$) and the estimator reacts sensitively and strongly to any measurement discrepancies $y - \hat{y}$. This latter limit is referred to as the large-gain limit. In the small-gain limit (SGL, $G \gg W$), a configuration based on the downstream measurement y is capable of controlling the unstable flow: The transfer function norm $\|T_{wz}\|$ is 5.489 and 2.823 depending on the parameter setting for ℓ . The unconstrained controller with $\ell \rightarrow 0$ naturally achieves a better performance, but in both cases progress is made towards the stabilization of the unstable flow. Including both s and y in the estimator does not change the performance outcome, since the upstream signal s is dismissed by the estimator; we achieve the same performance numbers. In the large-gain limit (LGL), with negligible signal contamination $G \ll W$, the control performance improves over the corresponding small-gain limit as the estimator is able to better detect the unstable state from y . When both signals y and s are taken into account, the unstable dynamics (due to y) and the noise-induced disturbances (due to s) are fully recovered and the optimal performance limit of full state-information control (FSC) is reached.

B. Amplifier flow

For the case of an amplifier flow, where we set $b = 0$, no global instability is observed and the perturbation dynamics is entirely determined by the upstream noise. We conduct the same performance analysis as before, however, only the large-gain limit for the controller, with the vanishing control cost penalty $\ell \rightarrow 0$, has to be considered. The absence of an instability causes a

no-action strategy in the small-gain limit, where control efforts are maximally avoided while still rendering the flow stable. For freely dispensable control ($\ell \rightarrow 0$), the full state-information control (FSC) strategy achieves the best possible result of $P = 0$, i.e., the incoming disturbances have been entirely suppressed and the performance signal z is identically zero.

For the partial state-information control (PSC), with an estimator providing the state information from local measurements, the small-gain limit (SGL) of the estimator produces a no-action control law. This is expected as the input signals are heavily corrupted by measurement noise ($G \gg W$) and the state vector $\hat{\mathbf{q}}$ cannot be reliably estimated, no matter the input signal(s); the performance measure is the same as for the uncontrolled case, $P = 1$. For the large-gain limit of the estimator, when the signal-to-noise ratio of the measurement signals s and y is large, the inclusion of the s signal from upstream results in optimal performance, i.e., the full state-information control (FSC) performance of $P = 0$. By choosing only the y signal as an input, we recover the (normalized) uncontrolled reference performance of $P = 1$. This is not surprising since, in a convective environment, the downstream sensor y provides information that arrives too late for the controller to act upon. As a consequence, the combined input signal (s, y) achieves again the full-state control performance $P = 0$, whereby the downstream y signal is ignored by the estimator and the upstream s signal is solely responsible for the optimal performance.

C. Conclusions from the model problem

Our simple model problem, mimicking the key features of oscillator and amplifier flows (depending on the strength of the feedback parameter b), revealed characteristics that influence the setup and performance behavior of flow control configurations. We summarize and expand on these characteristics below:

(i) For oscillator flows (with a global instability), the input signals have to provide information from the feedback zone. Sensor input upstream of this feedback zone is irrelevant for the design and operation of the compensator. While in our case the upstream edge of the feedback zone is given directly by our choice of model, for a realistic application of this design rule the point of maximum receptivity to upstream propagating information (e.g., by acoustic radiation in compressible flows) has to be determined to establish the extent of the feedback domain.

(ii) Flows with oscillator behavior are best controlled with an upstream-downstream sensor setup, which tends towards a pure feedback configuration, as the instability gets stronger and the inclusion of upstream noise information becomes less relevant.

(iii) In the large-gain limit of the estimator, equivalent to clear uncontaminated signals, an ideal full state-information control (FSC) performance can be achieved if both upstream and downstream sensors are included; the downstream sensor, however, is more critical for this success.

(iv) For amplifier flows (i.e., in the absence of a global instability), only the large-gain limit (LGL) for the controller has to be considered. The small-gain limit (SGL), with a high penalization of any control effort, will result in a no-action control law, yielding a natural stabilization of the flow.

(v) For the estimator design, the limit of a vanishing signal-to-noise ratio results in a zero Kalman gain (SGL) and, consequently, to a no-action control strategy. In this case, we recover the performance of the uncontrolled case.

(vi) For untainted signals ($G \ll W$), on the other hand, we obtain large Kalman gains (LGL) and a nonzero control effort. The input from the signal y downstream of the actuator is dismissed in the estimation, as its information arrives too late for appropriate control action. Rather, the upstream signal s carries the necessary information and yields a disturbance rejection strategy for the controller, together with a full state-information control (FSC) performance.

(vii) Flows with amplifier behavior are best controlled with an feedforward sensor-actuator setup; the downstream sensor y can be safely ignored without any ensuing loss in performance.

These findings will be relevant for the setup and the performance analysis of more complex flow situation, treated in this paper. Similar results have been obtained in a recent comprehensive study of actuator and sensor placement for the disturbance control in boundary layers [23].

LINEAR CONTROL OF OSCILLATOR AND AMPLIFIER FLOWS

The sensor placement, with respect to the actuator, and the incorporation of available sensor information into the overall compensator design can also be analyzed [21] by turning to the estimation problem, given by the system (6). We deduced that, for convectively dominated flows (small values of b), state estimation improves significantly when information is processed from the upstream sensor. To further demonstrate this, we assess the estimation error \mathbf{e} resulting from the downstream y and the upstream s sensor in the limit of vanishing feedback, i.e., for the limiting case of purely advecting flow. We first only consider the second column in \mathbf{C}_y , describing the downstream sensor y , and denote it by \mathbf{C}_y . Placing the sensor downstream of the actuator guarantees a nonzero transfer function between u and y , an argument that is often made in practice in favor of a feedback configuration. It can easily be shown that the discrete observability matrix for the downstream sensor is of full rank and, as a consequence, we have full control over the eigenvalues of the matrix $\mathbf{A} + \mathbf{L}_y \mathbf{C}_y$, which governs the estimation-error dynamics [see Eq. (6d)]. The control of these eigenvalues, however, can only ensure the long-time behavior of the estimation error. In convectively dominated systems (small b), information quickly becomes irrelevant as it propagates downstream and adjusting the eigenvalues of $\mathbf{A} + \mathbf{L}_y \mathbf{C}_y$ proves inadequate for ensuring proper estimator performance. Physically, information from y is ineffective for the estimator, since it is swiftly swept away. This can also be seen by computing the Kalman gain in the presence of noise w . Solving a discrete algebraic Riccati equation, using only \mathbf{C}_y , and evaluating the Kalman gain, we observe $\mathbf{L}_y = 0$ in the large-gain limit. Thus, information from the downstream sensor y in the limit of $b = 0$ (pure advection) does not enter the estimation problem, despite the full rank of the observability Gramian; as a consequence, the downstream sensor can safely be removed without effect.

We repeat the above analysis for the upstream sensor s by considering the first column of \mathbf{C}_y , which we denote by \mathbf{C}_s . Forming again the discrete observability matrix based on \mathbf{A} and \mathbf{C}_s , we detect a rank deficiency. Nonetheless, for $b = 0$ this placement can yield accurate state estimation. The corresponding Kalman gain for this sensor is given as $\mathbf{L}_s = (001000000000)^T$. Forming the composite matrix $\mathbf{A} + \mathbf{L}_s \mathbf{C}_s$ that governs the estimation error dynamics, we see that the estimation error \mathbf{e}_k is given by $(w_{k-1} w_{k-2} 0000000000)^T$, indicating that no estimation error is made anywhere downstream of the sensor location.

The above analysis of our simple system has shown that in convection-dominated flows a feedforward configuration with a sensor located upstream of the actuator is superior to a feedback configuration. This has been illustrated for the extreme case of pure advection. Realistic flows typically contain a variety of physical processes, with advection only being one part; therefore, a hybrid feedback and feedforward setup may be advantageous. Nevertheless, the above findings should provide a guide for the effective layout of flow control problems based on the relative presence of advection and global instabilities.

A supplementary result of this analysis concerns the suitability of information about the observability Gramian as a guiding principle and diagnostic tool for an effective sensor placement. It seems that, for advection-dominated flows, classical observability measures (the rank of the Gramian) yield misleading results and should be applied with caution. As we observed for our model problem, rank deficiency of the Gramian does not pose a problem, while a full rank of the Gramian does not give any guarantees. The question of an appropriate quantity describing sensor effectiveness for the estimation process in advection-dominated flows has been addressed before [21]: An alternative measure, introduced as the sensor's visibility length, has been proposed that determines the spatial range over which the input from the sensor can maintain a given estimation error. This criterion appears more fitting to fluid flows with strong advection, as the asymptotic nature of the observability Gramian seems incompatible with the short time scales of fast advection.

V. CONTROL OF OSCILLATOR FLOWS: A MODEL-BASED APPROACH

From our simple model equation we have learned that fluid systems with a strong internal downstream-to-upstream feedback and a global instability are best controlled by a feedback configuration. Information about the instability comes from the downstream sensor, which is

processed by a controller and passed to an upstream actuator. In general, oscillator flows undergo a supercritical Hopf bifurcation at a critical Reynolds number, become globally unstable, and establish limit-cycle behavior. An example of this type of flow behavior is the flow behind bluff bodies: The wake vortices show little sensitivity to the external random disturbances and the shedding frequency is hardly influenced by noise sources. The goal of control efforts is commonly the suppression of the linear instability, i.e., the preservation of the flow near the unstable equilibrium point by linear control strategies [18]. A far more challenging goal is the manipulation of the limit-cycle behavior; it requires a nonlinear model for the flow behavior and a nonlinear approach to flow control, in particular for strongly supercritical parameter choices. Within the scope of this article, we focus on the former control goal: the suppression of linear instabilities by linear control near the critical Reynolds number. To this end, we consider as a specific case of an oscillator the flow over an open square cavity at supercritical Reynolds numbers of $Re = 7500$ [see Fig. 3(a) for a sketch of the geometry]. Following the results from our 12×12 model system, we place one actuator upstream of the cavity and one sensor near the downstream cavity edge. Due to the presence of a dominating instability, the upstream sensor s of the model (furnishing information about the incoming perturbations) contributes little to the control; consequently, we eliminate this sensor in our control layout.

A. The need for model reduction

We could follow the two-step optimization outline mentioned in the previous section to design a controller and estimator for our linear model [see Eqs. (6)]. We notice, however, that the dimension of the compensator, in particular the dimension of the estimated state $\hat{\mathbf{q}}$, is equal to the dimension of the system to be controlled. While this is acceptable for small models or academic exercises, in practical and large-scale applications the compensator has to provide control information in real time. Only control signals that are computed efficiently and arrive in time to achieve their intended purpose are constructive in a feedback control setup. It is necessary then to reduce the dimensionality of the compensator without compromising its effectiveness in transforming measurement input into control output. By design, the compensator and full system have the same number of degrees of freedom; to ultimately design a reduced-order compensator, we thus have to reduce the dimensionality of the full system and formulate a compensator for this reduced-order system.

A common technique of model reduction is based on a Galerkin projection approach that represents the full state vector \mathbf{q} as a linear combination of a few coherent structures [24]. Denoting by \mathbf{V} a rectangular matrix whose columns consist of these structures, we can state that $\mathbf{q} \approx \mathbf{V}\bar{\mathbf{q}}$, where $\bar{\mathbf{q}}$ contains the coefficients of the linear combination. The columns of the matrix \mathbf{V} represent a basis in which we approximate the full-state dynamics. A second basis \mathbf{W} is necessary to perform the projection; it has to satisfy $\mathbf{W}^H\mathbf{V} = \mathbf{I}$, with \mathbf{I} as the identity matrix, i.e., it has to be biorthogonal to \mathbf{V} . Substituting this Galerkin expansion into the governing equations (3), we can formulate a reduced state-space system for the expansion coefficients $\bar{\mathbf{q}}$. The system matrix for this reduced system reads $\bar{\mathbf{A}} = \mathbf{W}^H\mathbf{A}\mathbf{V}$, the control matrix is $\bar{\mathbf{B}} = \mathbf{W}^H\mathbf{B}$, and the measurement matrix is $\bar{\mathbf{C}}_y = \mathbf{C}_y\mathbf{V}$.

While this projection provides a way to reduce the dimensionality of the full system to a size given by the number of coherent structures (columns in \mathbf{V} or \mathbf{W}), the question remains on how to select these structures to attain a valid reduced-order system that best approximates the original system during the subsequent compensator design procedure.

Figure 3, showing the ultimate closed-loop layout of the controlled system, suggests that during the model reduction process, the relation between the input u and the output y is most important. This relation is influenced by the instability of the flow as well as the stable dynamics. For the unstable part, it seems sensible to choose the unstable global modes (and their adjoints) as the coherent structures, or columns in \mathbf{V} (and \mathbf{W}), to represent the input-output behavior [16,17]. For the stable part, the choice is less obvious. In our case, we decide on balanced modes [25]; they represent structures that are equally observable and controllable and therefore best approximate the input-output behavior from u to y . Computationally, they are extracted from the impulse response from the actuator location

LINEAR CONTROL OF OSCILLATOR AND AMPLIFIER FLOWS

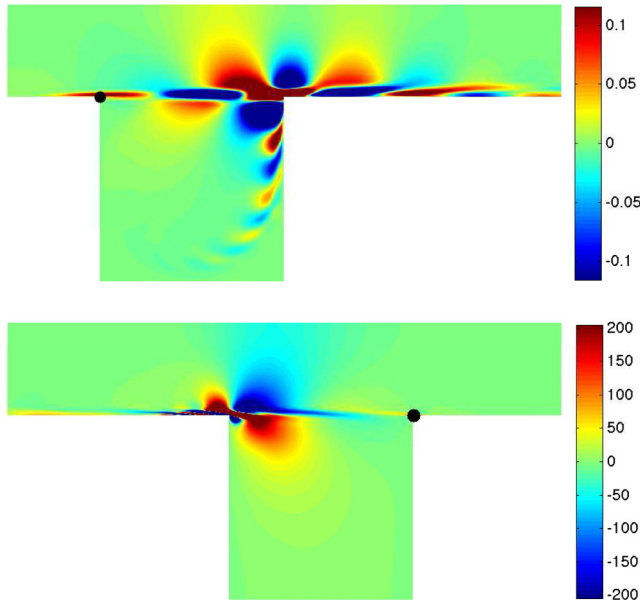


FIG. 7. Principal balanced mode (top) and its adjoint (bottom) for flow over an open cavity; contours of the streamwise velocity component are shown. The actuator and sensor locations are indicated by a black symbol.

and the adjoint impulse response from the sensor location by a snapshot technique [26–28] or other methods [29,30]. Special care has to be taken to eliminate components from the unstable dynamics during the impulse response simulations. Aligning all unstable global modes and the most dominant balanced modes as columns in \mathbf{V} and analogously the adjoint counterparts in \mathbf{W} , the reduced state $\bar{\mathbf{q}}$ consists of the amplitudes of the respective structures.

Figure 7 shows the principal direct and adjoint balanced modes. They show support near the sensor and actuator locations and span the shear-layer region on top of the cavity. Even visually they seem to well represent the flow dynamics between upstream input and downstream output. The fact that these structures are respectively focused near the downstream and upstream edges of the cavity can be attributed to the non-normality of the linearized Navier-Stokes operator.

To assess the quality of our model reduction effort and validate the choice of our expansion bases, we compute the transfer functions for the full and reduced models. Our single-input-single-output (SISO) configuration ensures that the transfer function is a scalar function. It is given by the Laplace transform of the linearized governing equations and reads, for input u and output y , $T_{yu}(\omega) = \mathbf{C}_y(i\omega - \mathbf{A})^{-1}\mathbf{B}$, with $i\omega$ denoting the Laplace variable. The transfer function for the reduced system \bar{T}_{yu} follows from using the reduced matrices $\bar{\mathbf{A}}, \bar{\mathbf{B}}, \bar{\mathbf{C}}_y$. We evaluate the transfer function for real forcing frequencies, i.e., $\omega \in \mathbb{R}$. The transfer function of the full system requires the inversion of a large matrix $i\omega - \mathbf{A}$ for each choice of ω . A computationally more efficient method consists of computing an impulse response from the actuator location u recorded at the sensor location y ; Fourier transforming this temporal signal yields the desired transfer function. As a quality measure of our model reduction we choose $\|T_{yu}(\omega) - \bar{T}_{yu}(\omega)\|_\infty$, which can be applied equally to stable and unstable configurations. For unstable systems, it enforces the unstable eigenvalues of the reduced and unreduced systems to coincide while imposing a close match for the stable subspace dynamics.

In Fig. 8 the absolute value of the full-system transfer function T_{yu} is displayed as a black dashed line. The peaks in the transfer function can be associated with a set of global modes describing the Kelvin-Helmholtz-type instabilities of the shear layer: For our chosen parameters, the lowest-frequency peak corresponds to a stable response, whereas the four subsequent peaks

PETER J. SCHMID AND DENIS SIPP

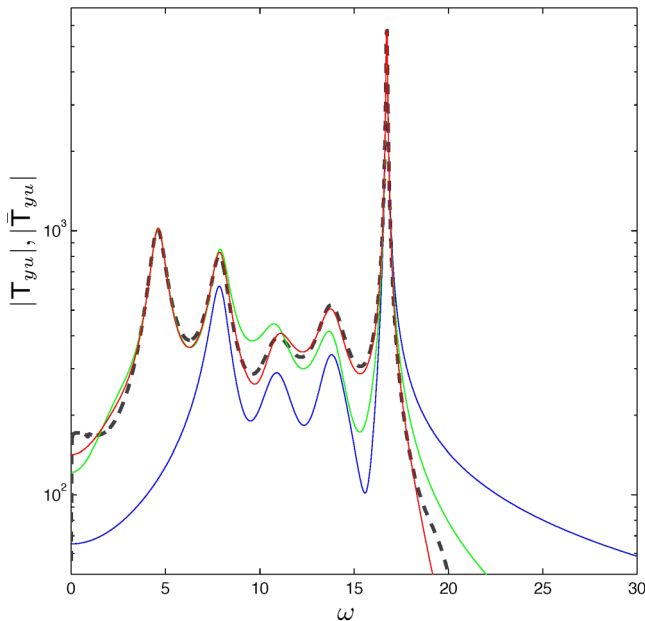


FIG. 8. Open-loop transfer function $|T_{yu}(\omega)|$ of the full plant (black dashed line) and of reduced-order models based on the four unstable global modes and no (blue), four (green), and eight (red) balanced modes to represent the stable subspace.

describe the global instability. Transfer functions of the reduced-order model are included as well. All underlying expansion bases \mathbf{V}, \mathbf{W} contain the four unstable global modes, but a varying number of balanced modes. If only the unstable global modes are used (blue line), the reduced-order transfer function deviates substantially from the full-system transfer function, even though there is an indication of all four unstable frequencies. As more balanced modes are added, the match improves rapidly. With eight balanced modes, in addition to the four unstable global modes, a very good match between the reduced-order and full-system transfer function could be achieved. This comparison highlights the fact that the stable subspace has to be represented properly for an effective model reduction of an oscillator system and, as a consequence, a successful controller. Even though the dynamics is dominated by the instabilities, information about the stable dynamics is equally required.

B. Design of a reduced-order compensator

With the Galerkin bases for the model reduction established, we can formulate the reduced-order equivalent of our fluid system. It describes the evolution of the coefficient vector $\bar{\mathbf{q}}$ driven by the control signal u and the external noise w ; measurements y are taken, which are assumed to be contaminated by measurement noise g . The cost objective is based on the performance sensor signal z .

Mathematically, we have

$$\dot{\bar{\mathbf{q}}} = \bar{\mathbf{A}}\bar{\mathbf{q}} + \bar{\mathbf{B}}u + \bar{\mathbf{B}}_w w, \quad (7)$$

$$y = \bar{\mathbf{C}}_y \bar{\mathbf{q}} + g, \quad (8)$$

$$z = \bar{\mathbf{C}}_z \bar{\mathbf{q}}. \quad (9)$$

We will use the above system in place of the full system to design a controller and estimator.

We proceed by designing an estimator that reconstructs an approximate state $\hat{\mathbf{q}}$ from the measurements y of the full system; this state $\hat{\mathbf{q}}$ constitutes an estimate of the state vector $\bar{\mathbf{q}}$ of

LINEAR CONTROL OF OSCILLATOR AND AMPLIFIER FLOWS

the reduced system. As mentioned before, the addition of a second driving term of the form $L(y - \hat{y})$ accomplishes this task. The estimator (Kalman filter) reads

$$\dot{\hat{\mathbf{q}}} = \bar{\mathbf{A}}\hat{\mathbf{q}} + \bar{\mathbf{B}}u + L(y - \hat{y}), \quad (10a)$$

$$\hat{y} = \bar{\mathbf{C}}_y\hat{\mathbf{q}}. \quad (10b)$$

The additional driving term accounts for the discrepancy between the true measurement y and the estimator-produced measurement \hat{y} [from Eq. (10b)] and the manner in which this discrepancy enters the equation for the estimated state is determined by the Kalman gain L . This gain follows from an optimization problem: We wish to minimize the variance of the estimation error $\mathbf{e} = \mathbf{q} - \hat{\mathbf{q}}$ while observing the governing equations (10). A variational formulation of this optimization problem produces the algebraic Riccati equation

$$\bar{\mathbf{A}}\mathbf{P} + \mathbf{P}\bar{\mathbf{A}}^H - \mathbf{P}\bar{\mathbf{C}}_y^H\mathbf{G}^{-1}\bar{\mathbf{C}}_y\mathbf{P} + \bar{\mathbf{B}}_w\mathbf{W}\bar{\mathbf{B}}_w^H = 0, \quad (11)$$

which has to be solved for the intermediate variable \mathbf{P} . The optimal Kalman gain can be determined via the algebraic expression

$$\mathbf{L} = \mathbf{P}\bar{\mathbf{C}}_y^H\mathbf{G}^{-1}. \quad (12)$$

In Eq. (11), covariances of two noise sources appear: the covariance of the system noise w denoted by $\mathbf{W} = \mathcal{E}(ww^H)$ and the covariance of the measurement noise g represented by $\mathbf{G} = \mathcal{E}(gg^H)$, where $\mathcal{E}(\cdot)$ stands for the expected value of its argument. It immediately becomes clear that the optimality of the Kalman gain L and, consequently, the performance of our estimator (in providing accurate approximations to the flow state from measurements alone) critically depend on our ability to furnish covariances of the noise sources that reliably reflect reality. Deterioration of the estimator is to be expected when the solution to the Riccati equation is based on incomplete or inaccurate noise covariances.

It is interesting to distinguish two limiting cases: (i) For $\mathbf{G}/\mathbf{W} \gg 1$, which corresponds to highly corrupted measurements or a relatively quiet noise environment, confidence in our model is high and the Kalman gain L is very low and (ii) for $\mathbf{G}/\mathbf{W} \ll 1$, which stems from either very accurate measurement signals or a strong influence of external noise sources, the corresponding Kalman gain L is very high, indicating that repeated sensing is necessary to arrive at sufficiently accurate estimates of the state.

For the design of the controller, we assume a proportional control law [31] of the form $u = \mathbf{K}\hat{\mathbf{q}}$. As was the case for the estimator, the control gain \mathbf{K} is the outcome of an optimization problem: We seek to minimize our cost objective subject to the governing equations. Furthermore, as before, a variational approach leads to an algebraic matrix Riccati equation for an auxiliary variable \mathbf{Q} given by

$$\bar{\mathbf{A}}^H\mathbf{Q} + \mathbf{Q}\bar{\mathbf{A}} - \mathbf{Q}\bar{\mathbf{B}}\ell^{-2}\bar{\mathbf{B}}^H\mathbf{Q} + \bar{\mathbf{C}}_z^H\bar{\mathbf{C}}_z = 0. \quad (13)$$

The optimal control gain \mathbf{K} follows from \mathbf{Q} via the algebraic expression

$$\mathbf{K} = -\ell^{-2}\bar{\mathbf{B}}^H\mathbf{Q}. \quad (14)$$

In the above, the commonly used quadratic cost functional $\mathcal{J} = \int_0^\infty |z|^2 + \ell^2|u|^2 dt$ has been used, where the user-specified parameter ℓ^2 imposes a balance between control performance $|z|^2$ and control cost $|u|^2$.

We notice that the Riccati equation (13) for the control problem is void of terms relating to noise sources; only the system and control matrices and the details of the cost objective enter the equation. We thus conclude that not the controller but the estimator is concerned with the influence of noise and uncertainty on the compensated system. Any deterioration in performance, or failure to control, in the presence of noise must be attributed to the estimator's inefficacy in recovering a sufficiently accurate state from measurements.

Finally, the combination of estimator and controller, i.e., the compensator, provides the reduced-order module that transforms the measurement signal from the full system into an optimal control

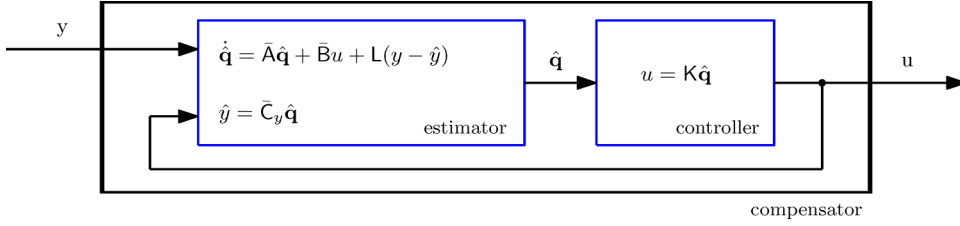


FIG. 9. Block diagram of the compensator consisting of estimator and controller.

signal. It is sketched as a block diagram in Fig. 9; the governing equations of each subunit are stated as well. This module is then attached to the reduced-order system, a procedure referred to as closing the loop. The closed-loop control problem, including true and estimated states, finally reads (in matrix form)

$$\begin{pmatrix} \dot{\hat{q}} \\ \dot{\bar{q}} \end{pmatrix} = \underbrace{\begin{pmatrix} \bar{A} & \bar{B}K \\ LC_y & \bar{A} - LC_y + \bar{B}K \end{pmatrix}}_{\bar{A}^{cl}} \begin{pmatrix} \bar{q} \\ \hat{q} \end{pmatrix} + \begin{pmatrix} \bar{B}_w w \\ Lg \end{pmatrix}. \quad (15)$$

By design, the composite closed-loop block matrix \bar{A}^{cl} is stable. With the system in closed-loop mode, the transfer functions from the noise sources w and g to the performance signal z provide a quality measure for the compensated system. The presence of a dominant instability argues for a comparatively small noise source, which allows for the design of the Kalman gain L in the small-gain limit. Similarly, by considering rather large control costs (large ℓ^2), also the control gain K can be determined for the small-gain limit. In these limits, we can assess the controller performance by inspecting the transfer function \bar{T}_{zg}^{cl} of the compensated system with measurement noise g as input and the performance measure z as output; in our case, we take the downstream sensor signal y to double as our performance measure z . The magnitude of this transfer function is displayed (by a black line) in Fig. 10. In the same figure, we also display (by a red line) the transfer function \bar{T}_{ug}^{cl} of the compensated system with again measurement noise g as input, but the control signal u as output. These transfer functions should be compared to the open-loop transfer function depicted (by the black dashed line) in Fig. 8.

At the end of the design procedure, the compensator dimension is identical to the reduced-order plant system, which can easily be deduced from Eq. (15). In terms of a block diagram, the design step for the reduced-order compensator is shown in Fig. 11(a). The motivation for the model reduction, however, has been the design of a low-dimensional compensator, which will ultimately be attached to the full-scale fluid system and provide control signals in real time [see Fig. 11(b)]. Residual degrees of freedom in the full system that have not been accounted for in the reduced-order system represent a perturbation of the closed-loop dynamics. It is imaginable that these perturbations cause a degradation of the control performance or even a failure (due to instability) of the closed-loop system. Hence, it is legitimate to investigate the effect of perturbations that originate from applying a compensator to a system it was not exactly designed for; the issue of robustness of the control design thus naturally arises.

C. Robustness

The combination of a full-state system and reduced-order compensator can be stated mathematically (in matrix form) as

$$\begin{pmatrix} \dot{\hat{q}} \\ \dot{\bar{q}} \end{pmatrix} = \underbrace{\begin{pmatrix} A & BK \\ LC_y & \bar{A} - LC_y + \bar{B}K \end{pmatrix}}_{A^{cl}} \begin{pmatrix} \bar{q} \\ \hat{q} \end{pmatrix} + \begin{pmatrix} B_w w \\ Lg \end{pmatrix}, \quad (16)$$

LINEAR CONTROL OF OSCILLATOR AND AMPLIFIER FLOWS

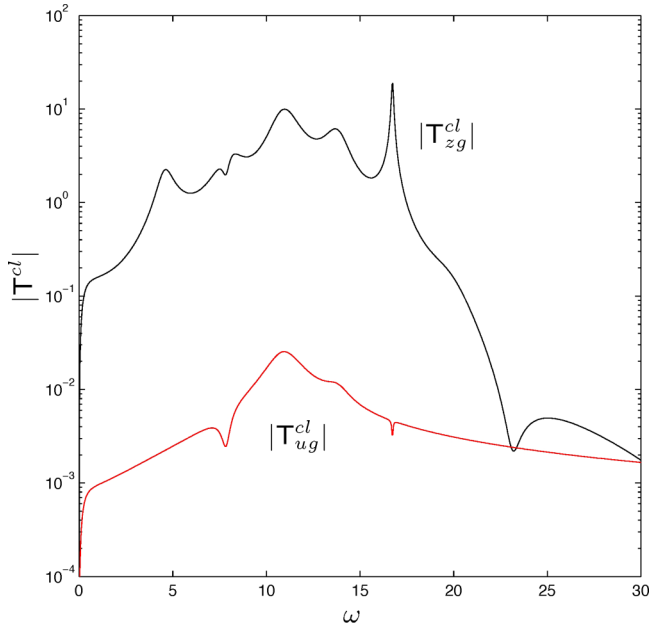


FIG. 10. Closed-loop transfer function $|T_{zg}^{cl}(\omega)|$ of the reduced plant from measurement noise g to performance sensor output z (in black) and from measurement noise g to control input u (in red).

where \mathbf{A} represents the large-scale system matrix with many degrees of freedom, while $\bar{\mathbf{A}}$ is our 16×16 reduced system matrix describing the dynamics in a space spanned by four unstable global modes (and their counterparts with negative frequencies) and eight balanced modes. We derive the closed-loop transfer function from the sensor noise g to the performance measure z as $T_{zg}^{cl} = T_{zu} \mathbf{K}_{uy} / (1 - T_{yu} \mathbf{K}_{uy})$, with T_{zu} and T_{yu} as the full-plant transfer functions (see Fig. 8) and \mathbf{K}_{uy} as the transfer function of the compensator given by $\mathbf{K}_{uy}(\omega) = \mathbf{K}(i\omega - \bar{\mathbf{A}} - \bar{\mathbf{B}}\mathbf{K} + \bar{\mathbf{L}}\bar{\mathbf{C}}_y)^{-1}\bar{\mathbf{L}}$. Closed-loop instabilities are to be expected when a pole of the transfer function T_{zg}^{cl} ventures into the unstable half plane, defined as $\mathbb{C}_+ \equiv \{z | \text{Re}(z) > 0\}$, or, equivalently, when unstable zeros appear in the denominator of T_{zg}^{cl} , i.e., $1 - T_{yu}(\omega)\mathbf{K}_{uy}(\omega)$. If there is no difference between the full-plant transfer function T_{yu} and its reduced analog \bar{T}_{yu} , then all zeros of $1 - T_{yu}(\omega)\mathbf{K}_{uy}(\omega)$ are stable by design and correspond to the eigenvalues of $\bar{\mathbf{A}}^{cl}$. Nonetheless, approximations and truncations have been made in the derivation of \bar{T}_{yu} and minor departures from the transfer function of the original system T_{yu} should be anticipated. Even a slight mismatch in the two transfer functions may induce an instability in the feedback loop and render the compensator ineffective. Quantifying this margin to instability is the purpose of a robustness analysis.

To this end, we modify the open-loop transfer function \bar{T}_{yu} of the reduced system and track its influence on the eigenvalues of the closed-loop system [32]. More specifically, we consider multiplicative changes of the form $\bar{T}_{yu} \rightarrow \xi \bar{T}_{yu}$, with $\xi \in \mathbb{C}$, and monitor the movement of zeros of $1 - \xi \bar{T}_{yu}(\omega)\mathbf{K}_{uy}(\omega)$ into the unstable half plane as ξ varies. The values of ξ where we observe these zero crossings provide critical gain margins when $\xi = a \in \mathbb{R}^+$ or critical phase margins when $\xi = e^{i\phi}$. Beyond these critical margins the closed-loop system will be unstable. From a physically perspective, the gain margin a is linked to an estimation error of the amplification rate of an instability and the phase margin ϕ represents an estimation error of its advection speed.

It is worth pointing out that robustness is most relevant when the open-loop transfer function T_{yu} is nonzero, i.e., in a feedback configuration when the control signal u affects the measurement y used

PETER J. SCHMID AND DENIS SIPP

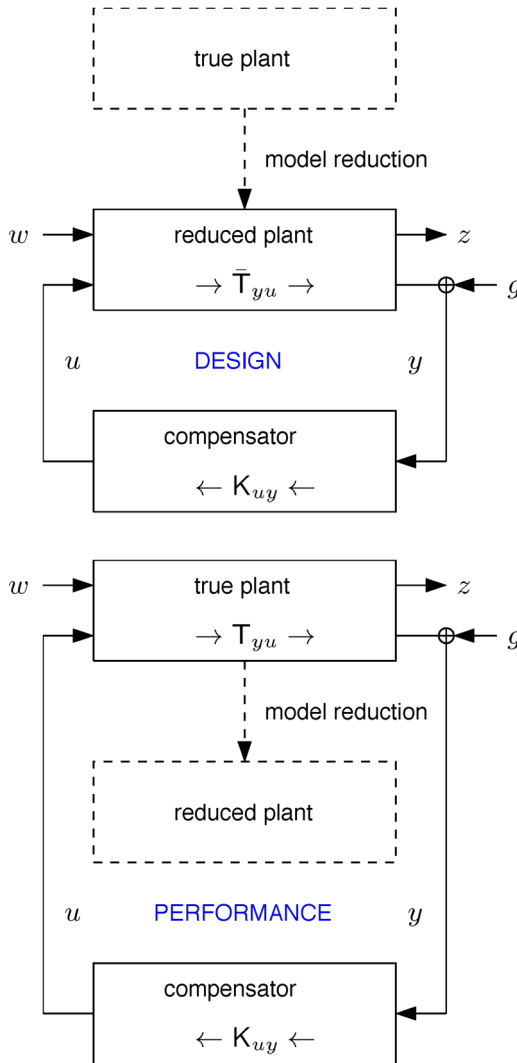


FIG. 11. Shown on top is the design of a compensator based on a reduced-order model of the true plant. Stability of this configuration is ensured by design. On the bottom is the application of the designed compensator to the full model of the true plant. Stability is not guaranteed; a robustness analysis can provide gain and phase margins for the occurrence of closed-loop instabilities.

in the estimator. As we have concluded from our simple 12×12 model, this is the proper layout for oscillator flows where a global structure destabilizes, synchronizes, and dominates the entire dynamics. For amplifier flows, which favor a feedforward setup with the measurement y upstream of the actuator u and hence $T_{yu} = 0$, a robustness analysis is nonessential.

As a reference case, we display the spectrum of the uncontrolled reduced-order system, i.e., the eigenvalues of \bar{A} ; see the blue symbols in Fig. 12, where only positive frequencies $\lambda_i > 0$ are shown. We verify the four unstable eigenvalues. Superposed on this spectrum are the eigenvalues of the compensated system \bar{A}^{cl} as red symbols. We have chosen $\ell \gg 1$, which heavily penalizes the control effort, together with $G/W \gg 1$; due to the resulting small values of K this limit is referred to as the small-gain limit. In this limit, control is focused on only the unstable modes, since further stabilizing

LINEAR CONTROL OF OSCILLATOR AND AMPLIFIER FLOWS

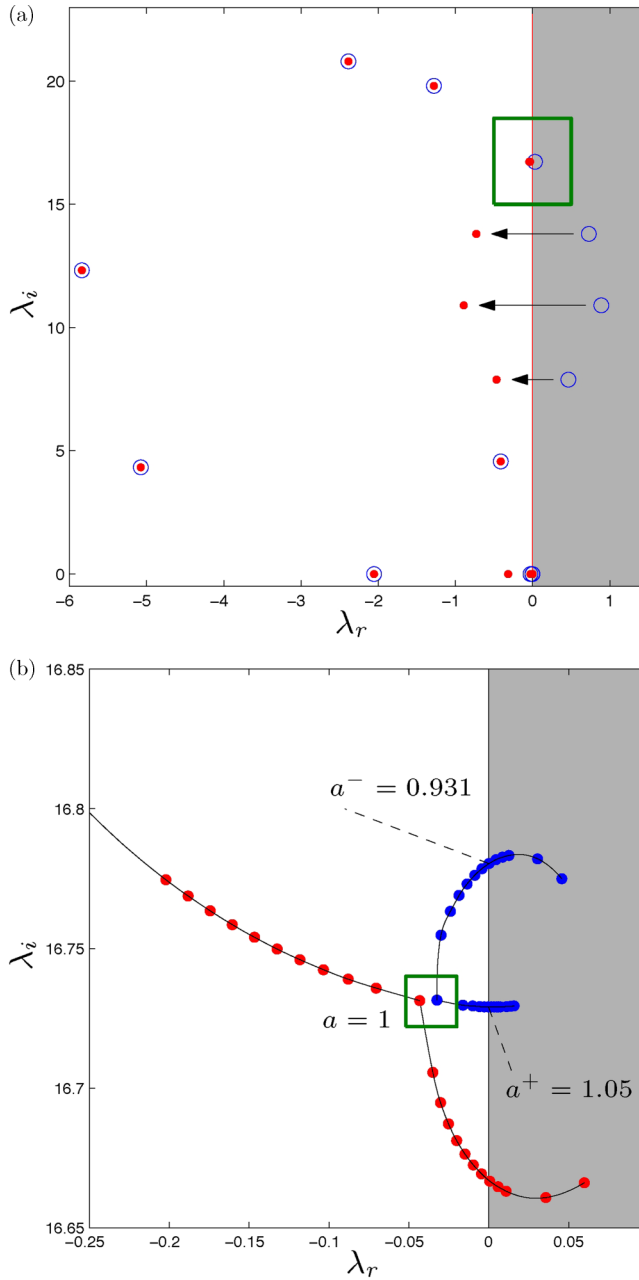


FIG. 12. (a) Eigenvalues of the uncontrolled reduced-order model (blue symbols) and of the compensated system (red symbols), showing the reflection of the (four) unstable eigenvalues into the stable half plane as well as the invariance of the (four) stable eigenvalues. (b) Robustness analysis: tracing the critical eigenvalues [indicated by the green box in (a)] as a function of $\xi = a \in \mathbb{R}^+$. The gain margins are given by $a^+ = 1.05$ and $a^- = 0.931$. For $0.931 \leq a \leq 1.05$ the compensated system is stable. The case $a = 1$ corresponds to the red eigenvalues inside the green box in (a).

stable modes would squander control energy and unnecessarily increase our cost objective. One can further show that in the small-gain limit, the unstable eigenvalues are simply reflected about the neutral line. Figure 12 verifies this phenomenon.

PETER J. SCHMID AND DENIS SIPP

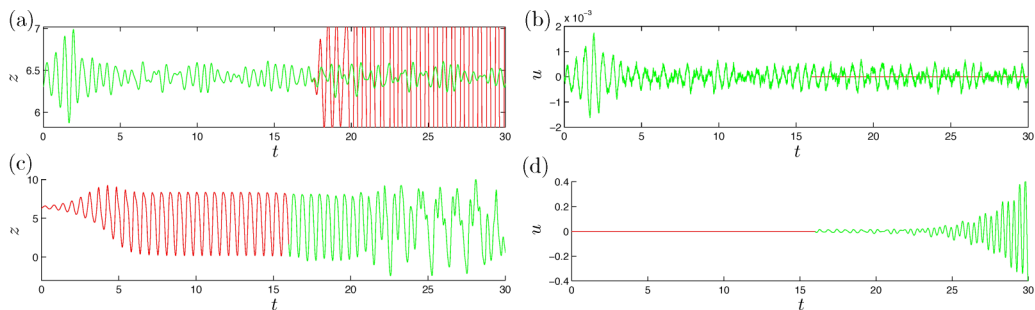


FIG. 13. Controller performance for flow over an open cavity. (a) Applying control to the system dynamics near the base flow, with corresponding control signal (b). (c) Applying linear control to the saturated limit-cycle behavior, with corresponding control signal (d).

Pursuing the robustness ideas introduced above, we investigate the change in eigenvalues of the compensated system as the multiplicative parameter ξ is varied. We will focus on one particular stabilized eigenvalue (indicated by the green box in Fig. 12) and probe its movement as $\xi = a \in \mathbb{R}^+$ increases from 0.75 to 1.5. In the special case $a = 1$, we recuperate the design situation, i.e., a stable compensated system.

As we detune the transfer function by premultiplying it by $0.75 \leq a \leq 1.5$, the eigenvalue traces an arclike curve that, for two critical values of a , crosses into the unstable (gray) half plane. We determine these critical values as $a^+ = 1.05$ and $a^- = 0.931$. For values of a within the interval $a^- < a < a^+$ we can guarantee stability of the closed-loop system; of course, this interval contains the design point for $a = 1$. The permissible gain margins, however, are rather narrow and indicate that only a 5% overprediction or 7% underprediction of the perturbation's amplification can be tolerated before the compensated system becomes unstable and ineffective. The phase margins, i.e., the robustness to errors in the estimated advection speed, can be determined in an analogous manner by choosing $\xi = \exp(i\phi)$. This analysis reveals a small phase margin of $\phi = \pm 3^\circ$ before closed-loop instabilities prevail, an equally bleak result.

D. Performance evaluation in full-plant mode

In spite of the rather narrow gain margin, we still anticipate a reasonable compensator performance as long as the mismatch between the full-plant transfer function T_{yu} and its reduced-order equivalent \bar{T}_{yu} is sufficiently small. We use direct numerical simulations of flow over the open cavity and choose as initial condition a superposition of the base flow and the least stable global mode with a small amplitude. The downstream sensor y , providing flow information to the estimator, is taken to be corrupted by Gaussian white noise of variance $G = 1$. We first consider the time interval from $t = 0$ to $t = 18$ in Fig. 13(a). A short transient period can be observed, after which the compensated performance signal z settles into an erratic oscillation whose variance and spectral content coincide with the behavior deduced from Fig. 10 (black curve); the control signal u shows an analogous behavior and validates the closed-loop transfer function in Fig. 10 (red curve). The compensator is switched off at $t = 18$, after which the performance measure z increases sharply and saturates into a limit cycle. This simulation demonstrates that our compensator is capable of maintaining the flow in the neighborhood of the equilibrium point.

A second simulation will test whether the same compensator can recover the equilibrium solution once the system has established a limit-cycle behavior. To this end, an uncontrolled simulation ($t = 0$ to 16) first leads to a limit cycle, after which, at $t = 16$, the compensator is activated. Again, we monitor the performance signal z and the control signal u . We see that the compensator is unable to stabilize the flow; increasingly larger control input is observed, without the intended effect on the performance measure z . We conclude by noting that a compensator with increased robustness

LINEAR CONTROL OF OSCILLATOR AND AMPLIFIER FLOWS

margins, e.g., using \mathcal{H}_∞ techniques [33,34], may have performed more gracefully. The design of such an improved compensator is beyond the scope of this article.

VI. CONTROL OF AMPLIFIER FLOWS: A DATA-DRIVEN APPROACH

For amplifier flows, where a global stability is absent and advection is the dominant transport process, our simple 12×12 model shows that the signal from the downstream sensor y becomes less and less important for the compensator, while the upstream sensor s provides the pertinent information for the control of incoming perturbations. The same absence of a global instability brings to the foreground the importance of modeling the noise environment and incorporating it into the control design, which is accomplished by basing the control of the flow on the sensor s closest to the noise source.

In this configuration, a formulation of the control problem based on a state-space model and its solution by Riccati equations [35] becomes ill adapted to the control layout. Moreover, the previous analysis for oscillator flows required the input of covariance information \mathbf{W} and \mathbf{G} together with information about the form of noise input \mathbf{B}_w to determine the optimal Kalman and control gains. In the presence of a (strong) global instability, this information has only a secondary influence on the ultimate control performance and thus modeling inaccuracies can be tolerated to a certain degree (even though robustness issues have to be considered). For stable configurations, the noise information becomes more important and imposes a far stronger influence on the control performance; the indispensability of an accurate noise model becomes the principal design handicap for amplifier flows.

A. Design of an input-output model

The block diagram of a compensated system in Fig. 9 demonstrated that the fluid system (i.e., the plant) is characterized by its transfer function from u to z under the influence of the two noise sources w and g . In the previous, model-based approach this transfer function has been implicitly given by a state-space formulation. The transfer from u to z thus occurs by u exciting a specific state vector \mathbf{q} , which is then measured at the performance sensor location yielding z . In other words, the state-space formulation represents the transfer function as a mapping from a low-dimensional input signal u to a low-dimensional output signal z via a high-dimensional state vector \mathbf{q} .

An alternative to this approach is to postulate a mapping between the low-dimensional signals by eliminating the high-dimensional state; the details of this mapping are then matched to observed sequences of input-output data. Mathematically, this approach can be motivated by the formal solution of (3) for zero initial condition $\mathbf{q}(0) = \mathbf{0}$, which reads

$$z = \int_0^t \underbrace{\mathbf{C}_z \exp[(t - \tau)\mathbf{A}]\mathbf{B}}_{h_{zu}(t-\tau)} u(\tau) d\tau + \int_0^t \underbrace{\mathbf{C}_z \exp[(t - \tau)\mathbf{A}]\mathbf{B}_w}_{h_{zw}(t-\tau)} w(\tau) d\tau. \quad (17)$$

In the above expression we replace the low-high-low-dimensional terms $\mathbf{C}_z \exp[(t - \tau)\mathbf{A}]\mathbf{B}$ and $\mathbf{C}_z \exp[(t - \tau)\mathbf{A}]\mathbf{B}_w$ by the low-dimensional temporal convolution kernels $h_{zu}(t - \tau)$ and $h_{zw}(t - \tau)$, respectively. The performance signal z can hence be represented by a time trace of input signals u and w appropriately weighted by the kernel functions h_{zu} and h_{zw} . These kernel functions implicitly carry information about the system dynamics \mathbf{A} , the control input \mathbf{B} , the noise input \mathbf{B}_w , and the measurement output \mathbf{C}_z . However, we do not formulate these kernel functions explicitly from the system matrices; we rather assume them as unknown and identify them by observing input and output data sequences.

For convenience (but without loss of generality), we convert (3) to a discrete-in-time system [36] describing the evolution of the state vector and performance measurement over a small, constant

time step Δt . We have

$$\mathbf{q}_{n+1} = \mathbf{A}\mathbf{q}_n + \mathbf{B}u_n + \mathbf{B}_w w_n, \quad (18a)$$

$$z_n = \mathbf{C}_z \mathbf{q}_n, \quad (18b)$$

where $\mathbf{q}_n = \mathbf{q}(n\Delta t)$ and similarly for the other time-dependent variables. In a slight abuse of notation, we label the discrete-form matrices in the above expressions by the same symbols as in the continuous case, even though they are different (but related). Motivated by the formulation (17), we express the discrete measurement signal z_n as a function of past control and past noise signals weighted by (yet unknown) coefficients $\{b_j\}, \{c_k\}$ according to

$$z_n + \sum_{i=1} a_i z_{n-i} = \sum_{j=0} b_j u_{n-j} + \sum_{k=0} c_k w_{n-k} + R. \quad (19)$$

In addition to the discrete convolution terms, we have introduced an autoregressive term for z_n (taking into account the history of the discrete z signal) with unknown coefficients $\{a_i\}$. By recording and processing sequences of u_n, w_n , and the resulting z_n we can fit the model output given by (19) to the observed measurement z_n by linear regression [37]. We encounter two difficulties with this approach: (i) In most cases, the noise input w cannot be determined to a sufficient degree of accuracy to yield an effective model and (ii) the residual error R for a linear-regression solution to (19) is assumed to be white. The first issue will be dealt with by replacing the true noise input w by the upstream sensor s [see Fig. 1(c)], which furnishes critical information about the incoming perturbation environment, also in accord with the conclusions drawn from our 12×12 model, which favors input about the noise from an upstream sensor for convectively dominated flows. Thus far, we then have

$$z_n + \sum_{i=1} a_i z_{n-i} = \sum_{j=0} b_j u_{n-j} + \sum_{k=0} c_k s_{n-k} + R. \quad (20)$$

The different paths of information, described by the above equation, are sketched in Fig. 14. The link between the control signal and the downstream sensor, quantified by the coefficients $\{b_j\}$, is indicated by (1); the link between s and z , described by $\{c_k\}$, is labeled by (2). By replacing the noise environment w by the upstream sensor signal s , we have to acknowledge that only the observable part of w can be captured by s ; see pathway (3) in Fig. 14. The remaining (unobservable) component passes through the system and directly impacts the measurement z downstream [represented by path (4)]. During the passage of this noisy component through the system, it gets modified according to the system's transfer function: certain frequency components will be amplified, others will be damped. As the modified signal arrives at the downstream sensor, it will resemble colored noise, irrespective of its original frequency distribution upstream. It seems incorrect then to assume the residual error R as white. For this reason, we model the residual error R by a moving-average term (with unknown coefficients) that can account for a colored residual noise spectrum. We thus propose

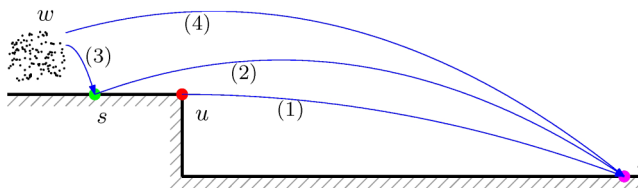


FIG. 14. Sketch indicating the transfer of information to be modeled by the ARMAX structure. Transfer of information (1) from the control u to the performance sensor z and (2) from the upstream sensor s to the performance sensor z ; (3) the observable part of the disturbance environment w measured by s and (4) the part of w unobservable by s but impacting the performance sensor z .

LINEAR CONTROL OF OSCILLATOR AND AMPLIFIER FLOWS

the revised model

$$z_n + \sum_{i=1} a_i z_{n-i} = \sum_{j=0} b_j u_{n-j} + \sum_{k=0} c_k s_{n-k} + \sum_{p=1} d_p R_{n-p} + R_n. \quad (21)$$

The additional coefficients $\{d_p\}$ are used to capture a temporal correlation in the error term and hence describe colored noise impacting the downstream sensor. The final model (21) is referred to as an ARMAX model: It consists of an autoregressive part for the measurement signal z , a moving-average part for R , and two exogeneous inputs for u and s .

B. Applying statistical learning

The final form of our input-output model (21) has been determined by combining the form of the exogeneous input (17) with physical arguments about the frequency content of residual errors. Now that the model has been established, we collect time sequences of the various signals as a learning data set to determine the coefficients $\{a_i\}$, $\{b_j\}$, $\{c_k\}$, and $\{d_p\}$. In the presence of (unknown) noise w we force the system by an input signal u , which has to be sufficiently rich in frequencies such that all relevant time scales of the fluid system are excited. We then gather, in a time-synchronous manner, the responses in s and z . The collection of these signals constitutes the learning data set. The set of unknown coefficients can be determined from this data set by a simple least-squares technique that matches the model output to the true output. With the coefficients determined, a second data set, the testing data set, is used to validate the generality of the identified ARMAX model by exposing it to input data that has not been part of the training set; effective models will nonetheless reproduce the correct output sequences.

The identification process is complex and dependent on many parameters. The intrinsic parameters of the model (such as the number of the various coefficients) can be determined from correlation analyses of the output and input signals (see [38] for details). The length of the learning samples is another parameter the user has to choose. Models with a high complexity or models determined from rather short data sequences often result in small errors for the learning data set but show large discrepancies when applied to the testing data set. This issue, referred to as overlearning, has to be avoided by finding a judicious compromise between the error norm from the learning and testing data sets [39].

For the backward-facing step, we force the system by an actuator signal u , shown in Fig. 15(b), and record the output signals in s and z , shown in Figs. 15(a) and 15(c), respectively. The signal in u consists of a sequence of finite-width pulses of various amplitudes; it has been selected to force a direct response in the downstream sensor z , while at the same time not masking the response of the downstream sensor to the noise environment (represented by the proxy signal s). The signal z shows the response both to the forcing in u (delayed due to advection) and to the signal s . The signal s appears rather stochastic and captures the observable part of the upstream noise.

Once the model has been identified from this learning data set, it is subjected to a different forcing u and the model-predicted output signal z_p is recorded. The signal z_p is then compared to the output signal z_t of the direct numerical simulation, which has been forced by the same input signal u . This comparison is displayed in Fig. 15(d). An initial transient is observed over a time span that corresponds to the approximate travel time of information between the s and z locations. After this transient period, the predicted and true downstream signals coincide, verifying that the system-identified ARMAX model is able to accurately predict the downstream signal z given the upstream measurement s and the control input u .

C. Design of a compensator by disturbance rejection

The identification of an input-output relation from the learning data set can be thought of as constructing a reduced-order model of the open-loop system. In the case of an oscillator flow, a reduced-order model has been designed directly from the state-space model by Galerkin projection onto a few flow-relevant structures; in the case of an amplifier flow, we postulated a low-dimensional

PETER J. SCHMID AND DENIS SIPP

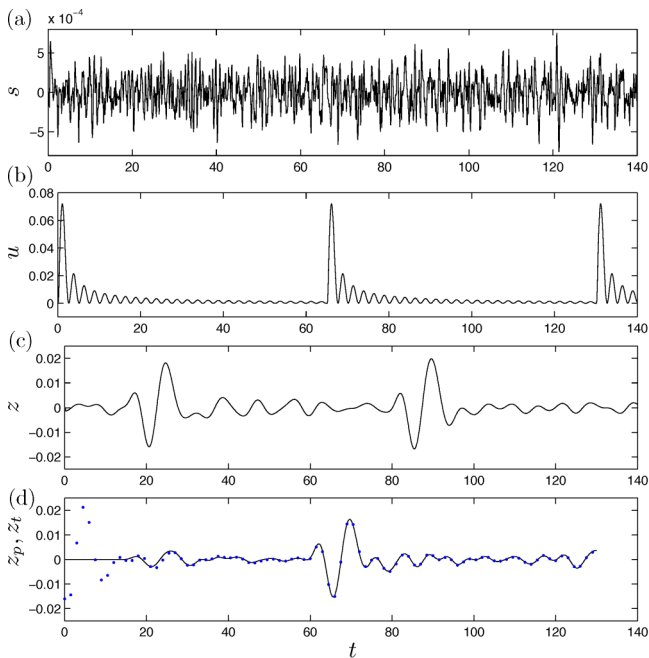


FIG. 15. Learning data set consisting of the recorded measurements from the (a) upstream sensor s , (b) input signal u , and (c) downstream performance sensor z . Note that a pulse in u (b) yields a pulse in z (c) after a time delay corresponding to the traveling time of a perturbation between the actuator and the performance sensor location. The validation of the model is shown in (d), where the predicted output (solid black line), for a forcing different from the learning set and for a different noise environment, is compared to the true signal (blue symbols) from the full system.

ARMAX model and determined its coefficients by observing and processing input-output data. In either case, the final result of the model reduction can be formulated in terms of an open-loop transfer function of the full fluid system.

In the next step, a compensator has to be designed. For the oscillator flow, this has been accomplished by solving two Riccati equations and combining the resulting estimator and controller. For amplifier flows, a compensator can be designed from the identified transfer function far easier by applying a concept known as disturbance rejection.

After some simple algebraic manipulations involving z transforms, we can reformulate the identified ARMAX model in the form $z = T_{zs}s + T_{zu}u$ using the two transfer functions from s to z and from u to z . The measurement z is our performance output and we seek to minimize this signal. By setting $z = 0$, the former expression directly yields a control law, namely, $u = -T_{zu}^{-1}T_{zs}s$. This law links upstream measurements s about the incoming perturbations to a control strategy u . The inverse of the transfer function T_{zu} should give us some pause, since this transfer function may be small or zero for certain frequencies, in which case the inversion would yield infinite or unacceptably large control gains. For this reason, the inversion is better to be performed by a Moore-Penrose pseudoinverse, which allows us to specify a lower threshold below which any control action is ignored. The pseudoinverse is equivalent to a regularization step and is needed to acquire effective control action. In effect, the threshold below which singular values are not inverted but rather ignored in the pseudoinverse allows us to process transfer functions T_{zu} that show stop-band behavior for given frequencies.

It is worth mentioning that the compensator can also be designed in the time domain. In this case, we need to decide on a time interval over which the performance signal z is to be minimized.

LINEAR CONTROL OF OSCILLATOR AND AMPLIFIER FLOWS

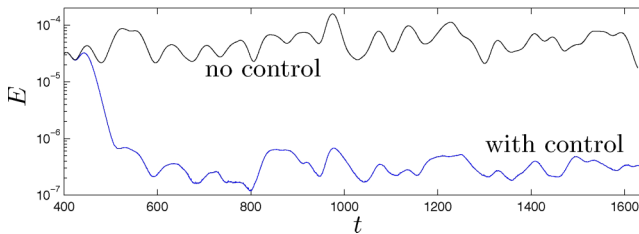


FIG. 16. Global perturbation energy versus time for the uncontrolled (black) and controlled (blue) cases; a reduction of two orders of magnitude is accomplished by applying feedforward flow control. The Reynolds number of the flow is $Re = 500$.

Also in this case, a regularized inversion has to be applied before a practical control law can be derived.

D. Performance of the compensator in full-plant mode

After a reduced-order model has been identified and a disturbance-rejection controller has been designed, we can apply the compensator to the direct numerical simulation. We extract information from the upstream sensor s and use the control strategy to act on the flow via the control signal u . The control strategy has been designed to optimally reduce the measurement signal z farther downstream and, strictly speaking, we cannot presume more than this imposed control objective. Nevertheless, we evaluate the total perturbation energy of the flow within the entire computational domain and compare the uncontrolled to the controlled case. Figure 16 displays the total perturbation energy as a function of time for the two cases. We observe a substantial reduction of the perturbation energy, of more than two orders of magnitude, corroborating the efficiency of the designed controller. This plot, however, does not give any indication of the spatial extent of our control result. More information can be gained by locally time averaging the perturbation energy. Figure 17 displays contours of the time-averaged perturbation energy for the controlled and uncontrolled cases, using the same color map for comparison. Without control, a localized region of high perturbation energy forms downstream of the base-flow reattachment point, with a peak at about 25 units from the step, which ultimately decays owing to the global stability of the flow. This energy peak is drastically decreased, once the control is switched on [see Fig. 17(b)]. In the controlled case, the peak of the locally-time-averaged perturbation energy has not shifted appreciably, but has diminished in amplitude by two orders of magnitude. It is remarkable that the locally-time-averaged perturbation energy could be reduced over a large extent of the computational domain downstream of the

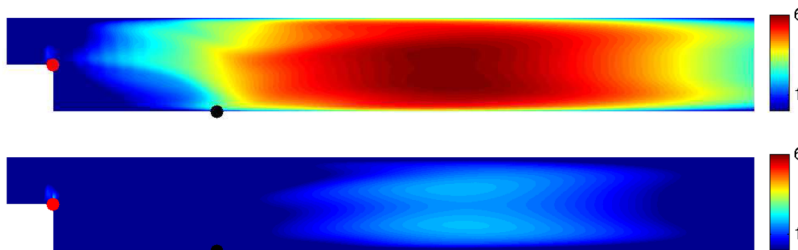


FIG. 17. Time-averaged local perturbation energy for the uncontrolled (top) and controlled (bottom) flow over a backward-facing step at $Re = 500$. The vertical coordinate has been scaled by a factor of 3; the controller location (red symbol) and objective sensor location (black symbol) are also indicated. Logarithmic contour levels have been used, with identical color maps.

PETER J. SCHMID AND DENIS SIPP

reattachment point, despite the fact that only a reduction of the measurement signal z (indicated by the black symbol in Fig. 17) has been used in the design of the compensator.

VII. SUMMARY AND OUTLOOK

In this article we considered the design and performance of linear control schemes for the manipulation of oscillator and amplifier flows. Two common flow configurations have been used: (i) the two-dimensional flow over an open cavity that, above a critical Reynolds number, is globally unstable and therefore acts as an oscillator flow and (ii) the two-dimensional flow over a backward-facing step that is globally stable but acts as an amplifier of external noise sources. In addition, a 12×12 model has been introduced that reproduced the main features of either flow configuration, simply by changing the strength of an intrinsic feedback loop. This model has been used to provide guidance in effective control setups for the two cases. It could be shown that oscillator flows are most appropriately controlled by a feedback configuration, while amplifier flows are best manipulated by a feedforward controller.

The decision about the control layout also dictates the tools to determine the transfer functions for the plant and the controller. In the case of an oscillator, a model-based approach has been taken that starts with a state-space formulation and yields two optimization problems involving Riccati equations. The resulting gains for the estimator and controller are combined into a compensator that uses measurements from the full system to determine a control strategy that is optimal in reducing a specified cost objective. The design process depends on our knowledge of two noise covariances (for the plant and measurement noise); however, in the presence of a dominant instability, we have enough latitude to approximate these covariances and still arrive at an effective control design. In the case of an amplifier, a data-driven approach using techniques from system identification [40] and statistical learning [39] is preferred. An underlying model, directly connecting control and measurement to performance output without passing through the state vector, can be postulated, with guidance from the governing equations. The unknown coefficients of this model are then determined by a statistical-learning approach, i.e., by fitting the model predicted to the true output. Any noise contamination in the processed data is thus reflected and accounted for in the identified coefficients. The controller for this model is straightforwardly designed by a disturbance-rejection argument. Both approaches, model-based design for oscillators and data-driven design for amplifiers, managed to achieve the prescribed cost objective.

The physical behavior inherent in the flow determines not only the control setup, but also sets bounds on what can be achieved by control efforts. As a critical component in this effort, the degree of internal feedback, quantifying the strength of an instability or the amplification gain of environmental disturbances (the parameter b in our model equation), plays an important role in the design and performance evaluation of the compensated system. In this sense, the flow physics substantially influences the degree of control success.

For the examples and configurations in this article, the optimal control resembles rather closely opposition control, with an account for advective motion via a delay. Identified structures (from an instability or arising from upstream noise via selective amplification) are opposed by nearly destructive interference from the actuator. This type of control action is a consequence of our performance-based control objective: lowering the kinetic energy of flow perturbations. Other choices for the cost functional or imposed side constraints may yield control strategies that deviate from opposition. To further study the effect of control on the flow physics, we need to study the compensated system and its coherent structures (modes); in the case of amplifier flows, the transfer functions will contain this information.

Robustness is an issue of great importance in the design of control systems [41]. It is concerned with sensitivity of the performance measure to changes in the design components. For feedforward control, robustness is ensured; for feedback control, it has to be quantified. Multiplicative detuning of the system transfer function produces gain and phase margins that set boundaries for a stable closed-loop system. The control design in this article has focused purely on performance measures.

LINEAR CONTROL OF OSCILLATOR AND AMPLIFIER FLOWS

The robustness analysis of the final design has been performed as an *a posteriori* diagnostic. It appears more fitting to incorporate robustness measures, together with performance measures, directly in our cost objective rather than evaluating them as an afterthought. In this way, we would determine a control law that shows good, albeit reduced, performance over a reasonable range of internal changes to our system. This type of control strategies is of practical importance, when modest performance, even off the design point, is more desirable than optimal performance that rapidly deteriorates for even slight deviations from the design point. The design of robust flow control strategies is beyond the scope of this article and is left for future investigations.

An alternative approach to the robustness problem is given by adaptive control strategies [42,43], such as the FXLMS algorithm. Rather than determining a fixed control law, a proper actuator response is identified from sensor input, based on an approximate model for the flow behavior. In this setup, the performance sensor z is used to directly adjust the transfer function from the upstream sensor to the actuator. This type of compensator shows encouraging performance as well as significant robustness margins.

The techniques in this article are applicable to fluid system in the vicinity of an equilibrium point and the control laws have been designed to steer, as best as possible, any deviating flow back towards this point. We also learned that this linear control law becomes ineffective once the flow departs too far from the equilibrium point and settles into a nonlinear limit cycle. In order to control limit-cycle behavior, a nonlinear underlying model and a nonlinear control strategy are required. Following the system-identification approach in this article, we can postulate a nonlinear reduced-order model (e.g., using a proper orthogonal decomposition (POD)-based Galerkin projection [44,45]) motivated by the Navier-Stokes equations and determine the unknown coefficients of this model by matching the predicted output to the true output. Once verified by a testing data set, this model can be incorporated into a nonlinear model-predictive framework and used to manipulate limit-cycle behavior. In this manner, we attempt to control oscillator flows that have settled in the nonlinear regime.

Flow control techniques will continue to play an important role in fluid dynamics as we seek improved performance, reduced environmental impact, and increased operational ranges in fluid devices. By using techniques adapted to the inherent flow behavior, effective and efficient strategies can be designed to achieve these goals.

ACKNOWLEDGMENTS

The many discussions and contributions of Alexandre Barbagallo, Aurelien Hervé, Fabien Juillet, and Nicolas Dovetta are gratefully acknowledged.

-
- [1] B. J. Bayly, S. A. Orszag, and T. Herbert, Instability mechanisms in shear-flow transition, *Annu. Rev. Fluid Mech.* **20**, 359 (1988).
 - [2] Y. S. Kachanov, Physical mechanisms of laminar-boundary-layer transition, *Annu. Rev. Fluid Mech.* **26**, 411 (1994).
 - [3] P. J. Schmid and D. S. Henningson, *Stability and Transition in Shear Flows* (Springer Verlag, New York, 2001).
 - [4] A. Fedorov, Transition and stability in high-speed boundary layers, *Annu. Rev. Fluid Mech.* **43**, 79 (2011).
 - [5] S. Candel, D. Durox, T. Schuller, J.-F. Bourgoïn, and J. P. Moeck, Dynamics of swirling flames, *Annu. Rev. Fluid Mech.* **46**, 147 (2014).
 - [6] A. P. Dowling and A. S. Morgans, Feedback control of combustion oscillations, *Annu. Rev. Fluid Mech.* **37**, 151 (2005).

- [7] M. P. Juniper and L. Magri, Application of receptivity and sensitivity analysis to thermoacoustic instability, in *Progress in Flow Instability Analysis and Laminar-Turbulent Transition Modeling*, edited by E. Valero and F. Pinna, VKI Lecture Series 2014-05 (VKI, Sint-Genesius-Rode, 2014).
- [8] E. Strumberger, S. Günter, and C. Tichmann, MHD instabilities in 3D tokamaks, *Nucl. Fusion* **54**, 064019 (2014).
- [9] E. J. Strait, Magnetic control of magnetohydrodynamic instabilities in tokamaks, *Phys. Plasmas* **22**, 021803 (2015).
- [10] E. H. Dowell and K. C. Hall, Modeling of fluid-structure interaction, *Annu. Rev. Fluid Mech.* **33**, 445 (2001).
- [11] C. H. K. Williamson and R. Govardhan, Vortex-induced vibrations, *Annu. Rev. Fluid Mech.* **36**, 413 (2004).
- [12] O. Marquet, D. Sipp, and L. Jacquin, Sensitivity analysis and passive control of cylinder flow, *J. Fluid Mech.* **615**, 221 (2008).
- [13] S. Skogestad and I. Postlethwaite, *Multivariate Feedback Control* (John Wiley & Sons, New York, 1996).
- [14] S. S. Collis, R. D. Joslin, A. Seifert, and V. Theofilis, Active flow control: theory, control, simulation, and experiment, *Prog. Aerosp. Sci.* **40**, 237 (2004).
- [15] J. Kim and T. R. Bewley, A linear systems approach to flow control, *Annu. Rev. Fluid Mech.* **39**, 383 (2007).
- [16] A. Barbagallo, D. Sipp, and P. J. Schmid, Closed-loop control of an open cavity flow using reduced-order models, *J. Fluid Mech.* **641**, 1 (2009).
- [17] S. Ahuja and C. W. Rowley, Feedback control of unstable steady states of flow past a flat plate using reduced-order estimators, *J. Fluid Mech.* **645**, 447 (2010).
- [18] L. N. Cattafesta, Q. Song, D. R. Williams, C. W. Rowley, and F. S. Alvi, Active control of flow-induced cavity oscillations, *Prog. Aerosp. Sci.* **44**, 479 (2008).
- [19] D. Sipp and A. Lebedev, Global stability of base and mean flows: a general approach and its applications to cylinder and open cavity flows, *J. Fluid Mech.* **593**, 333 (2007).
- [20] A. Barbagallo, G. Dergham, D. Sipp, P. J. Schmid, and J.-C. Robinet, Closed-loop control of unsteadiness over a rounded backward-facing step, *J. Fluid Mech.* **703**, 326 (2012).
- [21] F. Julliet, P. J. Schmid, and P. Huerre, Control of amplifier flows using subspace identification techniques, *J. Fluid Mech.* **725**, 522 (2013).
- [22] X. Garnaud, L. Lesshafft, P. J. Schmid, and P. Huerre, Modal and transient dynamics of jet flows, *Phys. Fluids* **25**, 044103 (2013).
- [23] B. A. Belson, O. Semeraro, C. W. Rowley, and D. S. Henningson, Feedback control of instabilities in the two-dimensional Blasius boundary layer: The role of sensors and actuators, *Phys. Fluids* **25**, 054106 (2013).
- [24] E. Åkervik, J. Høpfner, U. Ehrenstein, and D. S. Henningson, Optimal growth, model reduction and control in a separated boundary-layer flow using global eigenmodes, *J. Fluid Mech.* **579**, 305 (2007).
- [25] B. Moore, Principal component analysis in linear systems: controllability, observability, and model reduction, *IEEE Trans. Autom. Control* **26**, 17 (1981).
- [26] K. Willcox and J. Peraire, Balanced model reduction via the proper orthogonal decomposition, *AIAA J.* **40**, 2323 (2002).
- [27] C. W. Rowley, Model reduction for fluids, using balanced proper orthogonal decomposition, *Int. J. Bifurcat. Chaos* **15**, 997 (2005).
- [28] G. Dergham, D. Sipp, J.-C. Robinet, and A. Barbagallo, Model reduction for fluids using frequential snapshots, *Phys. Fluids* **23**, 064101 (2011).
- [29] Z. Ma, S. Ahuja, and C. W. Rowley, Reduced-order models for control of fluids using the eigensystem realization algorithm, *Theor. Comput. Fluid Dyn.* **25**, 233 (2010).
- [30] S. J. Illingworth, A. S. Morgans, and C. W. Rowley, Feedback control off low resonances using balanced reduced-order models, *J. Sound Vib.* **330**, 1567 (2011).
- [31] S. S. Joshi, J. L. Speyer, and J. Kim, A systems theory approach to the feedback stabilization of infinitesimal and finite-amplitude disturbances in plane poiseuille flow, *J. Fluid Mech.* **332**, 157 (1997).
- [32] J. B. Burl, *Linear Optimal Control: H_2 and H_∞ Methods* (Addison-Wesley, Reading, 1999).

LINEAR CONTROL OF OSCILLATOR AND AMPLIFIER FLOWS

- [33] J. C. Doyle, K. Glover, P. P. Khargonekar, and B. A. Francis, State-space solutions to standard H_2 - and H_∞ -control problems, *Trans. Automat. Control* **34**, 831 (1989).
- [34] G. Vinnicombe, *Uncertainty and Feedback: \mathcal{H}_∞ Loop Shaping and the v -Gap Metric* (Imperial College Press, London, 2000).
- [35] S. Bagheri, L. Brandt, and D. S. Henningson, Input-output analysis, model reduction and control of the flat-plate boundary layer, *J. Fluid Mech.* **620**, 263 (2009).
- [36] A. C. Antoulas, *Approximation of Large-Scale Dynamical Systems (Advances in Design and Control)* (SIAM, Philadelphia, 2005).
- [37] S.-C. Huang and J. Kim, Control and system identification of a separated flow, *Phys. Fluids* **20**, 101509 (2008).
- [38] A. Hervé, D. Sipp, P. J. Schmid, and M. Samuelides, A physics-based approach to flow control using system identification, *J. Fluid Mech.* **702**, 26 (2012).
- [39] G. Dreyfus, J.-M. Martinez, and M. Samuelides, *Apprentissage Statistique* (Editions Eyrolles, Paris, 2011).
- [40] L. Ljung, *System Identification: Theory for the User*, 2nd ed. (Prentice Hall, Englewood Cliffs, 1998).
- [41] T. R. Bewley and S. Liu, Optimal and robust control and estimation of linear paths to transition, *J. Fluid Mech.* **365**, 305 (1998).
- [42] N. Fabbiane, O. Semeraro, S. Bagheri, and D. S. Henningson, Adaptive and model-based control theory applied to convectively unstable flows, *Appl. Mech. Rev.* **66**, 060801 (2014).
- [43] N. Fabbiane, B. Simon, F. Fischer, S. Grundman, S. Bagheri, and D. S. Henningson, On the role of adaptivity for robust laminar flow control, *J. Fluid Mech.* **767**, 094104 (2015).
- [44] B. R. Noack, K. Afanasiev, M. Morzynski, G. Tadmor, and F. Thiele, A hierarchy of low-dimensional models for the transient and post-transient cylinder wake, *J. Fluid Mech.* **497**, 335 (2003).
- [45] E. Caraballo, J. Little, M. Debiasi, and M. Samimy, Development and implementation of an experimental-based reduced-order model for feedback control of subsonic cavity flows, *J. Fluids Eng.* **129**, 813 (2007).